Peer-reviewed version available at *Int. J. Mol. Sci.* **2020**, *21*, 366; doi:10.3390/ijms21010366

Article

Hup-type hydrogenases of purple bacteria: homology modeling and computational assessment of biotechnological potential

Azat Vadimovich Abdullatypov [1,*]

[1] Institute of Basic Biological Problems of the Russian Academy of Sciences - a separate subdivision of PSCBR RAS (IBBP RAS), Pushchino, Moscow region, Russia; azatik888@yandex.ru

* Correspondence: azatik888@yandex.ru; Tel.: +7-(4967)-73-27-91

Abstract: Three-dimensional structure of six closely related hydrogenases from purple bacteria has been modeled by combining template-based and *ab initio* modeling approach. The results lead to conclusion that there should be 4Fe3S-cluster in the structure of these enzymes. Thus, these hydrogenases could drive attention for exploring their oxygen tolerance and practical applicability in hydrogen fuel cells. Analysis of 4Fe3S-cluster's microenvironment showed intragroup heterogeneity. Possible function of the C-terminal part of the small subunit in membrane binding has been discussed. Comparison of the built models with existing hydrogenases of the same subgroup (membrane-bound oxygen-tolerant hydrogenases) has been carried out. Analysis of intramolecular interactions in the large subunits showed statistically reliable differences in number of hydrophobic interactions and number of ionic interactions. Molecular tunnels were mapped in the models and compared with structures from PDB. Protein-protein docking showed that these enzymes could exchange electrons in oligomeric state, which is important for oxygen-tolerant hydrogenases. Molecular docking with model electrode compounds showed mostly the same results as with hydrogenases from *E.coli, H. marinus, R. eutropha, S. enterica;* some interesting results were shown in case of HupSL from *Rba. sphaeroides* and *Rvx. gelatinosus.*

Keywords: hydrogenases; hydrogen fuel cells; homology modeling; FeS clusters; transmembrane helices; molecular docking; molecular tunnels

1. Introduction

Purple bacteria are widespread organisms possessing tremendous potential for practical application. They are producers of many valuable compounds, such as photosynthetic pigments (carotenoids [1] and bacteriochlorophyll [2]), storage compounds (polyhydroxyalkanoates[3]), phytohormones [4] and molecular hydrogen [5]. Another promising application of purple bacteria is their use for enzyme production. For example, there is already one enzyme available on the market, namely 3-hydroxybutyrate-dehydrogenase, from *Rhodobacter sphaeroides* [6], which is used for analytical quantifications of 3-hydroxybutyrate and acetoacetate; beside these enzymes, purple non-sulfur and sulfur bacteria possess hydrogenase

enzymes. This group of enzymes has been studied for almost nine decades since their discovery by Stephenson and Stickland [7].

For example, Hyd-type hydrogenases from purple sulfur bacteria (*Chromatium vinosum (Allochromatium vinosum)* and *Thiocapsa roseopersicina*) have been used in hydrogen electrodes, which could act as components of fuel cells and hydrogen biosensors [8-9] . These enzymes are relatively oxygen-tolerant and thermostable. Nevertheless, they are reversibly inhibited in presence of low oxygen concentrations, although other studies demonstrated their oxygen tolerance in some experimental conditions [10-12]. Anyway, they lack clear determinants of oxygen stability described for other groups of hydrogenases. Since a fuel cell should be suitable for storage on air and operation in hydrogen, meaning that there could be steps of exposition of hydrogenase electrode to hydrogen-oxygen mixture, it gives rise to some obstacles for wide application of these enzymes in hydrogen electrodes.

On the other hand, there are hydrogenases demonstrating higher levels of oxygen tolerance than HydSL enzymes from *Thiocapsa roseopersicina* and *Chromatium vinosum*. Such enzymes are hydrogenases from *Hydrogenovibrio marinus*, *Ralstonia eutropha*, *Salmonella enterica* and hydrogenase-1 from *Escherichia coli.* According to X-ray crystallographic and electrochemical studies, these hydrogenases possess a 4Fe-3S cluster capable of reducing the oxidized active site by electrons from FeS clusters of adjacent hydrogenase molecule from a dimer of heterodimers [13-16].

Purple bacteria are known to possess specific hydrogen-sensing hydrogenases which were demonstrated to be absolutely insensitive to presence of molecular oxygen or air in hydrogen gas, as well as to acetylene [17]. However, hydrogen-sensing hydrogenases are the least active enzymes of this class, oxidizing only 5-20 μmol H_2 per mg protein per minute, which is apparently due to narrowness of gas access channels, thus low activity is inevitable price to be paid for absolute oxygen tolerance [18].

However, there is another group of hydrogenases in purple bacteria, namely HupSL-hydrogenases [19-24]. They haven't driven much attention as *in vitro* catalysts for a while, but recently discovered 4Fe3S-clusters lead to supposal that they should be treated as possible oxygen-tolerant hydrogen oxidation catalysts like the mentioned membrane-bound hydrogenases. Hence, their modeling appeared to be interesting in the prospect of their biotechnological application.

HupSL hydrogenase from purple sulphur bacterium *Thiocapsa roseopersicina* was modeled long ago by Szilagyi and colleagues [25]; moreover, it was studied experimentally. It was considered as unstable and oxygen-sensitive, but experimental conditions did not exclude proteolysis factor: the protein was isolated only as a fraction of DEAE-chromatogram of crude cell extract, which lost almost all its activity at 4 °C under air [26]. There was a proposal that the reason for its instability is low number of intersubunit ionic pairs [25].

Hydrogenase from *Rhodobacter capsulatus* was studied by a number of research teams. It was shown to participate in recycling of hydrogen produced in nitrogenase reaction. Among the *in vitro* studies, work of Magnani and colleagues should be noted. They demonstrated the possibility of existence of two binding sites for

electron acceptors (methylene blue and benzyl viologen), and diphenylene iodonium was shown to be an inhibitor of electron transfer to both methylene blue and benzyl viologen, but only in the second case the inhibition was complete [27]. Such multiplicity of electron acceptor binding sites should be taken into account when designing electrochemical devices based on such enzymes.

Rhodopseudomonas palustris CGA009 was shown to be a HupSL-defective strain uncapable of growing on H_2 as a sole electron donor. Genome sequencing revealed that it is caused by defective HupUV-sensing hydrogenase, particularly, by frame shift mutation in HupV gene. However, other strains of *Rps. palustris* have functional HupV gene and corresponding ability to utilize hydrogen in nitrogen-fixing conditions provided by HupSL hydrogenase [22].

Other enzymes studied in the current work are described in Discussion section.

The goals of the current work were as follows: 1) To obtain homology models of hydrogenases from six purple bacteria, *Thiocapsa roseopersicina, Rhodobacter capsulatus, Rhodobacter sphaeroides, Rhodopseudomonas palustris, Rubrivivax gelatinosus, Rhodospirillum rubrum*; 2) To study microenvironment of the proximal FeS clusters; 3) To assess intrasubunit and intersubunit interactions between amino acid residues in these enzymes; 4) to assess the possibility of membrane binding of the C-terminal extensions of the small subunits; 5) To map intramolecular tunnels (possible pathways of hydrogen and oxygen delivery to the active site); 6) to assess the possibility of their oligomerization into complexes providing electron exchange between the small subunits; 6) To perform molecular docking of model electrode compounds, namely graphene oxide and neutral red oligomers, in order to estimate their applicability in fuel cell electrodes compared to the membrane-bound hydrogenases from *E. coli, R. eutropha, H. marinus, S. enterica.*

2. Results

2.1. Modeling of main (aligned) parts of the hydrogenase enzymes; overview of modeling results

Several procedures were carried out to improve the quality of homology models built in MODELLER (see Methods section). One of the most valuable impacts into the overall quality of the models according to z-DOPE assessment [28] was made by energy minimization on YASARA web server [29-30].

Despite the high levels of homology of all the studied enzymes with X-ray crystallographic data, normalized DOPE z-scores comparable to those of template structures (3RGW, 3UQY) could not be obtained. However, z-score levels were below -1, meaning significant confidence level.

The results of homology modeling of all the studied hydrogenases confirm the presence of 4Fe-3S clusters in the position proximal to the active site. Generally, homology modeling positioned FeS-atoms of the built models close to corresponding cysteine residues, and the cysteine residues of models and templates could be superposed quite well. However, some artifacts occured such as rotation of cysteine SH groups from the Fe atoms. Figure 1 shows an example of such a problem that appeared during modeling the small subunits.

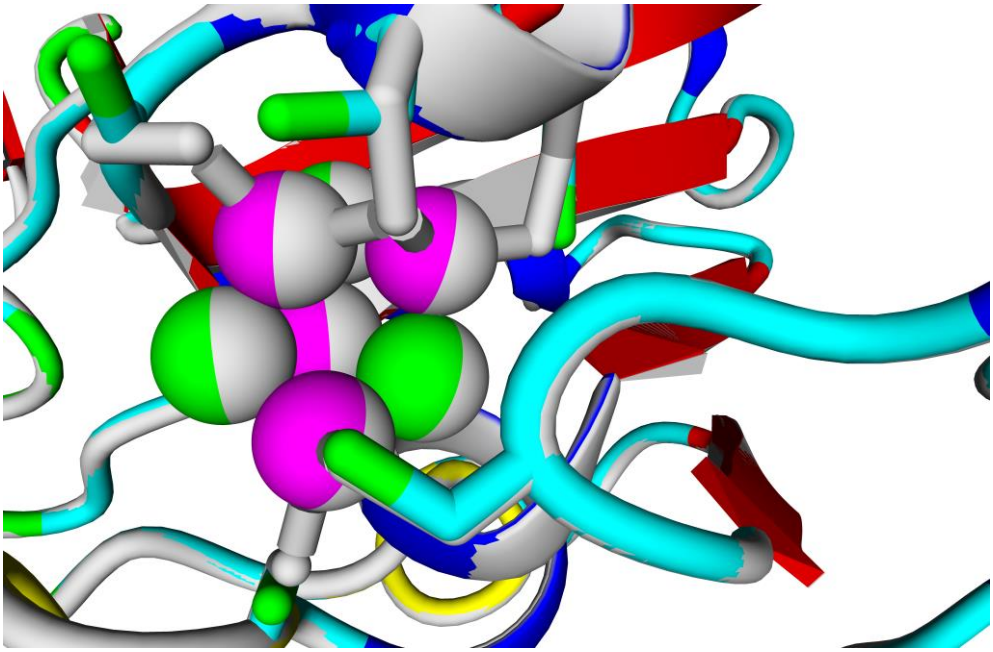

Figure 1. Superposition of hydrogenases from *Rhodobacter capsulatus* (model, this work) and *Ralstonia eutropha* (X-ray structure, PDB ID: 3RGW). In *Rhodobacter capsulatus* hydrogenase, iron is shown as magenta balls, inorganic sulfur is shown as green balls, protein carbon atoms are shown as cyan sticks, protein sulfur is shown as green sticks. *Ralstonia eutropha* hydrogenase molecule is all colored gray.

This problem can be solved either by constraining the dihedral angle around Cα-Cβ atoms of cysteine residue or by manual rotation of the cysteine residue after modeling; nonetheless, the combination of primary and tertiary structure alignment gives quite a definite evidence on the same structure of proximal FeS-cluster as in *E. coli* hydrogenase-1 or HoxKG-hydrogenases of *R. eutropha* and *Hv. marinus*, because six cysteines in corresponding positions (oriented similarly in space, not just in primary structure) instead of four cysteines in "classic" hydrogenases (like NiFe-hydrogenases of sulfate reducing bacteria or *Allochromatium vinosum*) must reduce the number of inorganic sulfur required to coordinate iron by 1, since the valence of inorganic sulfur (S^{2-}) equals 2, while valence of cysteinyl group ($-CH_2-S^-$) equals 1.

Other Fe-S clusters, medial and distal, do not differ significantly from the clusters of "classic" hydrogenases.

2.2. Microenvironment of proximal FeS-cluster

When considering the oxygen tolerance provided by 4Fe3S-cluster, one should always keep in mind that the nature of its microenvironment could possibly affect its ability to reduce the oxidized active site.

First of all, one of the most important residues in the small subunit is glutamic acid residue. All the studied hydrogenases possess very conservative motif, 73-LAVE-76 (numbering according to HupS from *Thiocapsa roseopersicina*, mature form). The residue E76 corresponds to E76 residue that was shown to shift closer to the iron atom during interaction with oxygen [31]. This residue's sidechain was close to Fe atoms (around 4.5 Å) in all the studied models.

Preprints (www.preprints.org) | NOT PEER-REVIEWED | Posted: 6 December 2019 doi:10.20944/preprints201912.0083.v1

Peer-reviewed version available at Int. J. Mol. Sci. 2020, 21, 366; doi:10.3390/ijms21010366

The multiple alignment of the large subunits of the studied hydrogenases with known oxygen-tolerant enzymes was more heterogenic (red color shows difference from HoxG/HyaB/HydB, green color shows identity):

```
>Thiocapsa roseopersicina HupL      -68-WAFTERICGVC-78|222-YGGKNPHP-229
>Rhodobacter capsulatus HupL        -68-WAFTERICGVC-78|223-FGGKNPHP-230
>Rhodobacter sphaeroides HupL       -67-WAFTERICGVC-77|222-FGGKNPHP-229
>Rhodopseudomonas palustris HupL    -69-WAFTQRICGVC-79|223-YGGKNPHP-230
>Rubrivivax gelatinosus HupL        -68-WAFVERICGVC-78|223-FGGKNPHP-230
>Rhodospirillum rubrum HupL         -68-WAFTQRICGVC-78|222-FGGKNPHP-229
>Hydrogenovibrio marinus HoxG       -69-WAFVERICGVC-79|224-FGGKNPHP-231
>Ralstonia eutropha HoxG            -68-WAFVERICGVC-78|223-FGGKNPHP-230
>Escherichia coli HyaB              -69-WAFVERICGVC-79|223-FGGKNPHP-230
>Salmonella enterica HydB           -69-WAFVERICGVC-79|223-FGGKNPHP-230
>Aquifex aeolicus HydA              -55-WAFTQRICGVC-65|231-FGGKNPHP-238
```

Figure 2. Microenvironment of the FeS clusters of the studied hydrogenases shown in multiple sequence alignment of large subunits. The amino acids found mainly in oxygen-tolerant hydrogenases are coloured green; those found in oxygen-sensitive hydrogenases are coloured red. NB: despite the presence of TQ-motif, hydrogenase from Aquifex aeolicus is also oxygen-tolerant.

It is interesting to note several things. First of all, only four of the six studied enzymes possess both residues highlighted by Bowman et al. as determinants of oxygen stability (measured experimentally as the reversibility of current after injection of oxygen into hydrogen feeding hydrogenase electrode), glutamate E73 and histidine H229 [16].

Moreover, only one of the studied hydrogenases has a valine residue which is conservative for the crystallized oxygen-tolerant hydrogenases, whereas other purple bacteria have more hydrophilic threonine residue instead. The role of this residue should also be investigated, because this residue is present in corresponding position in oxygen-sensitive hydrogenases of sulfate-reducing bacteria.

According to Bowman et al., substitutions of glutamate residues to alanine led to significant drop of oxygen stability; however, little is known about substitutions of this residue to glutamine, although it seems to be able to affect the electrochemical behaviour of the FeS cluster.

So, two polar variants can be selected among the modeled hydrogenases: hydrogenase from *Rubrivivax gelatinosus* is the one resembling well-known oxygen-tolerant membrane-bound hydrogenases like HoxKG from *Ralstonia eutropha (Alcaligenes eutrophus, Cupriavidus necator)*; hydrogenase from *Rhodopseudomonas palustris* has the maximal degree of difference from such hydrogenases (Figure 3).

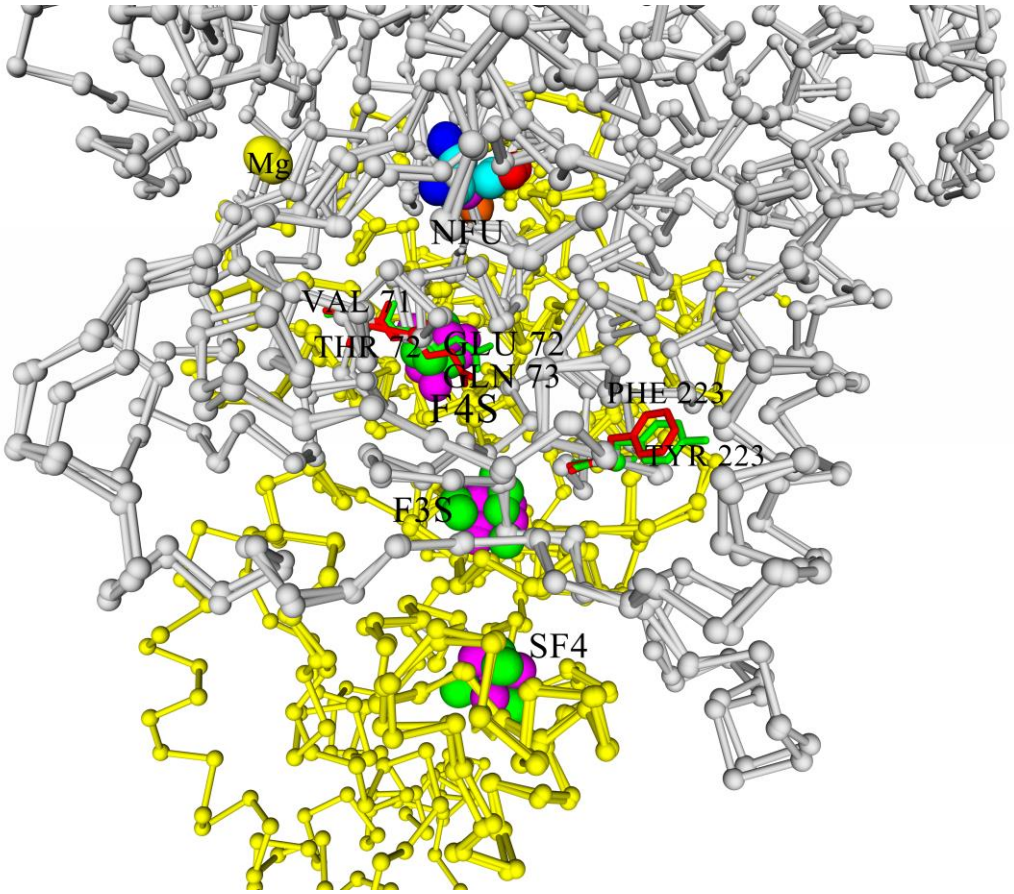

Figure 3. Microenvironment of the clusters of the studied hydrogenases: superposition of hydrogenases from *Rhodopseudomonas palustris* and from *Rubrivivax gelatinosus*. Most of the atoms of the active site (NFU) and FeS clusters are coloured by YASARA element colouring scheme: iron, magenta; sulfur, green; carbon, cyan; oxygen, red; nitrogen, blue. Nickel atom is coloured orange, magnesium atom (Mg) is yellow. The large subunits are colored gray, the small subunits are yellow the residues specific for "oxygen-tolerant" hydrogenases are coloured green (in HupSL from *Rvx. gelatinosus*), the ones specific for "oxygen-sensitive" enzymes are shown in red (in HupSL from *Rps. Palustris*). Conservative histidine residue is coloured blue. F4S - proximal 4Fe3S cluster; F3S - medial 3Fe4S cluster; SF4 - distal 4Fe4S cluster.

The three residues differing in those two hydrogenases (or residue pairs) can be arranged in a series according to the decrease of their possible effect on the electrochemical properties of the clusters and thus the oxygen tolerance. The first one should be E/Q: its side-chain is only 10 Å from the closest iron atom of 4Fe3S-cluster, as well as from the active site. So, the presence or absence of carboxylic group close to the proximal cluster looks like a factor affecting oxygen tolerance.

The following residue pair in the series is V/T: it is farther from the active site and 4Fe3S-cluster (11,5-12,5 Å when measured from the differing (methyl or hydroxyl) heavy atom) and its action could hardly be explained so explicitly.

The last pair is F/Y. It is 20 Å from the mentioned redox ligands and 16-17 Å from the medial 3Fe4S-cluster, when counted by the closest carbon of aromatic group.

Preprints (www.preprints.org) | NOT PEER-REVIEWED | Posted: 6 December 2019 doi:10.20944/preprints201912.0083.v1

Peer-reviewed version available at Int. J. Mol. Sci. 2020, 21, 366; doi:10.3390/ijms21010366

Beside the physical or at least geometrical basis, there should be statistical confirmation of the statement about the possibility of mediation of oxygen tolerance by certain residues.

Analysis of large subunits from HydDB database (group 1d) [32] showed that when aligning 215 amino acid sequences from 1d group, 214 of them contained 68-WAFVERICGVC-78 motif or its homolog (numbering as in PDB file of HoxKG from *Ralstonia eutropha*, 3RGW); one sequence was possibly just a fragment. In this consensus, the following amino acids were on corresponding positions (See Figure4; the exact number of amino acids on each position is given in Supplementary Table 1.):

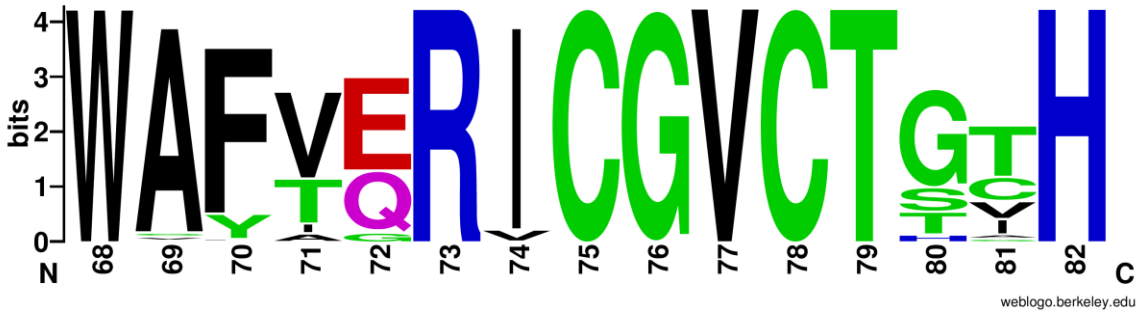

Figure 4. Sequence logo of large subunit consensus for hydrogenases from HydDB database (214 of 215 sequences, residues from 68 to 82). Hydrophobic residues are shown in black, amides are shown in magenta, other hydrophilic neutral residues are shown in green, negatively charged residues are shown in red, positively charged residues are shown in blue. Ordinate shows information content of the alignment positions in bits ($\log_2 20 = 4.321928$ if the residue is absolutely conservative)

As for the second conservative sequence (223-FGGKNPHPNYLVGG-236), the occupancies of the positions look as follows (detailed numbers in Supplementary Table 2):

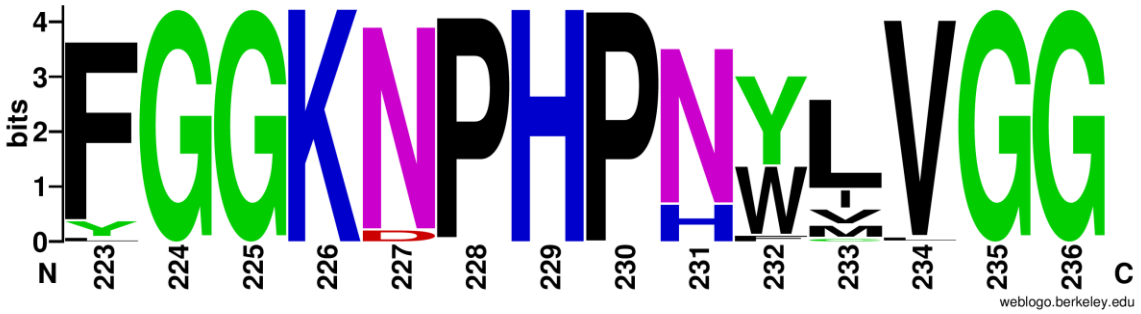

Figure 5. Sequence logo of large subunit consensus for hydrogenases from HydDB database (215 sequences, residues from 223 to 236). Hydrophobic residues are shown in black, amides are shown in magenta, other hydrophilic neutral residues are shown in green, negatively charged residues are shown in red, positively charged residues are shown in blue. Ordinate shows information content of the alignment positions in bits ($\log_2 20 = 4.321928$ if the residue is absolutely conservative)

Although the residues specific for the crystallized oxygen-tolerant hydrogenases (V71, E72, F223) really prevail in the group, the first two of them are present in not so overwhelming majority to be called "absolutely required" for oxygen tolerance. But the results of Bowman et al. showed that E73A substitution in *S. enterica* hydrogenase-5 led to appearance of irreversible component in the process

of inhibition of hydrogenase electrode by oxygen, whereas the native enzyme demonstrated almost 100% restoration of activity. On the other hand, the aforementioned hydrogenase from *Aquifex aeolicus* does also possess 4Fe3S-cluster (supernumerary cysteines in the small subunit), but it has a bit different sequence in the large subunit, WAFTQRICGVC [16].

2.3. C-termini of the small subunits

The C-termini of the small subunits comprise alpha-helical motifs. Their hydropathicities vary, but for all the studied hydrogenases there could be observed an increase of hydrophilicity from N-terminus to C-terminus of the C-end fragment.

To test the ability of the C-end fragments to form transmembrane anchors, they were analyzed on TMHMM Server 2.0 [33]. The analysis showed that clear tendency to form a transmembrane helix could be observed in *Rhodobacter capsulatus, Rhodobacter sphaeroides, Rhodopseudomonas palustris, Rhodospirillum rubrum*, and this helix appears to be from the 15th to the 37th residue of the selected hydrogenase fragments. The multiple aligment of their C-termini is shown below (Figure 6).

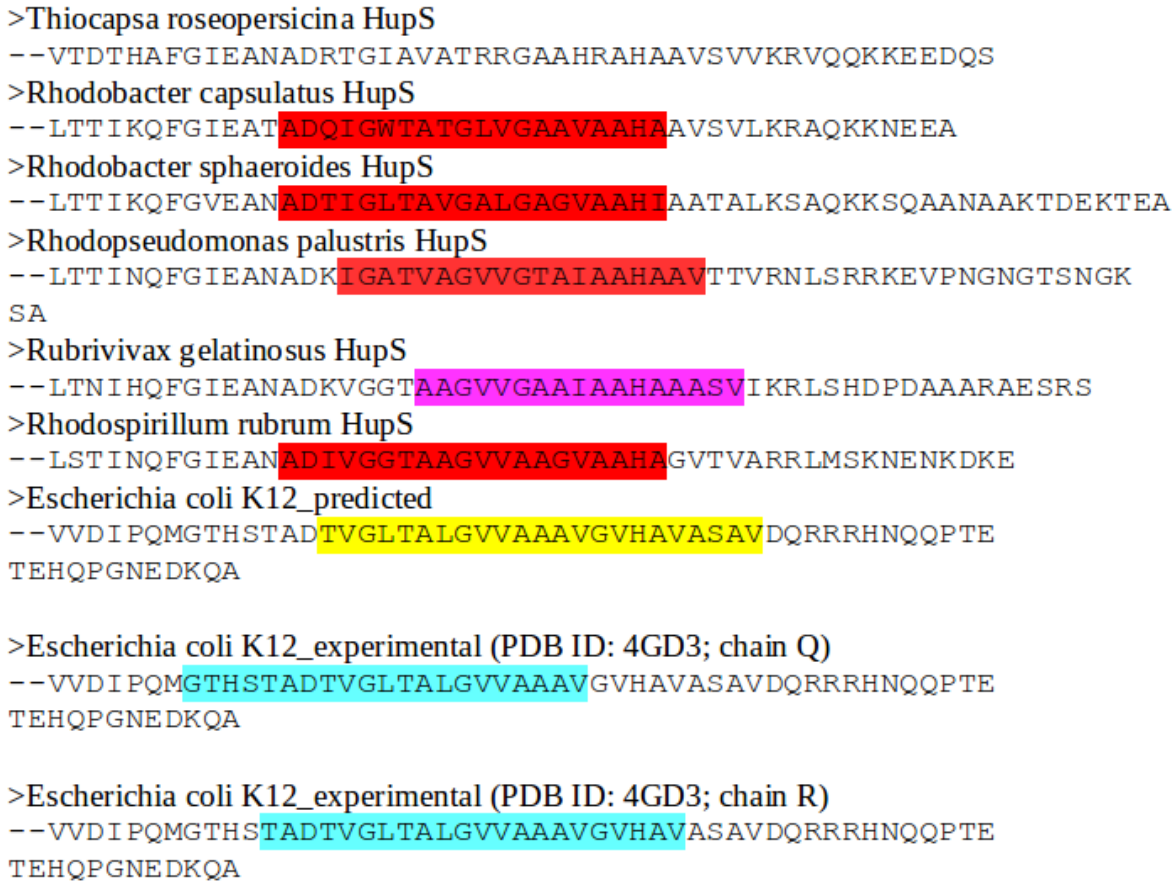

Figure 6. Predicted transmembrane helices in the modeled hydrogenases are highlighted in red; a region in *Rubrivivax gelatinosus* showing a slight transmembrane propensity is colored magenta (explanation below); predicted helix in *E.coli* is highlighted in yellow, and experimentally shown alpha-helices are colored cyan.

The results of the alignment with *Escherichia coli* hydrogenase-1 (PDB ID: 4GD3, 1G94 [34-35]) showed that the level of identity is too low to model the C-termini via homology modeling; the prediction of transmembrane helices by TMHMM server showed around 70% of overlapping of predicted and experimentally shown helices for *E.coli*, which can be reasonable enough to use the data of TMHMM server as information confirming the transmembrane orientation of the helices of the modeled hydrogenases. In case of hydrogenase from *Rubrivivax gelatinosus*, a region showed the probability to be a transmembrane alpha-helix higher than outside or inside part of the protein; but the values were low (below 0.6), whereas for *Rhodobacter*, *Rhodopseudomonas*, *Rhodospirillum* and *E.coli* they were above 0.8. It is interesting to note that substitution of four arginine residues in *Thiocapsa roseopersicina* to corresponding uncharged residues from *Rhodobacter* (Q, L, V, A) makes the server predict transmembrane helix in the derived variant as well. As for *Rubrivivax gelatinosus*, substitution of just a single lysine residue to alanine or isoleucine led to prediction of transmembrane helix there. The geometry of C-terminal fragments extracted from full-size models of the enzymes is shown on Figure 7.

Preprints (www.preprints.org) | NOT PEER-REVIEWED | Posted: 6 December 2019 doi:10.20944/preprints201912.0083.v1

Peer-reviewed version available at Int. J. Mol. Sci. 2020, 21, 366; doi:10.3390/ijms21010366

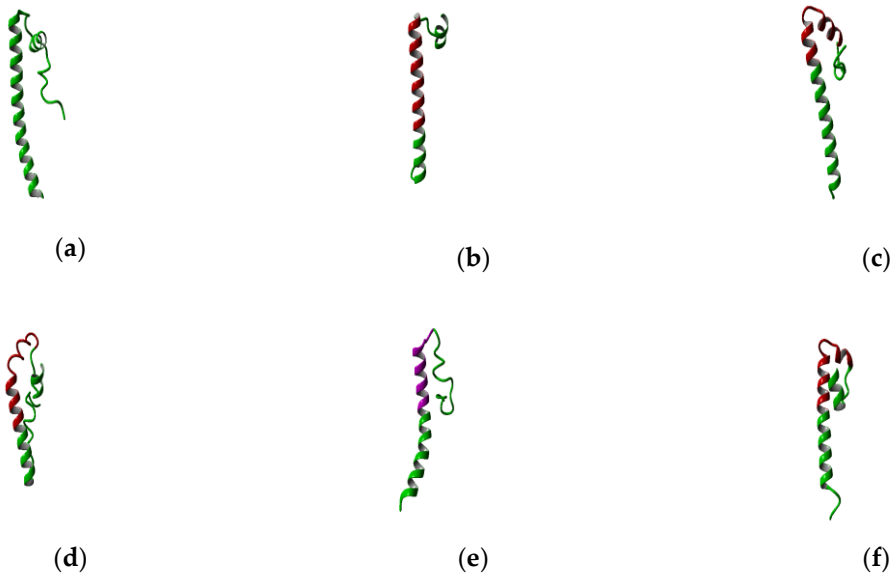

Figure 7. C-terminal parts of the small subunits of the hydrogenases (extracted from final full-size models, see below). Regions corresponding to predicted transmembrane helices are coloured red. Corresponding region of HupSL from Rubrivivax gelatinosus is coloured magenta. The C-termini of the helices are positioned in the bottom of each figure. The panels of the figure correspond to the following enzymes: **(a)** HupS from *Thiocapsa roseopersicina;* **(b)** HupS from *Rhodobacter capsulatus*; **(c)** HupS from *Rhodobacter sphaeroides*; **(d)** HupS from *Rhodopseudomonas palustris*; **(e)** HupS from *Rubrivivax gelatinosus*; **(f)** HupS from *Rhodospirillum rubrum*.

The possibility of formation of transmembrane helices is disputable, since three of four of these helices were broken during modeling (20 ns simulations in water before using as templates), which can evidence on the labile links in the moieties of the C-terminal fragments. Probably, presence of glycine residues makes these helices unstable. Another possibility could be the prediction error of TMHMM server itself, which was confirmed for the case of *E. coli* hydrogenase. The length of the predicted transmembrane helices (20 Aa) is enough to pass across the entire membrane.

It must be admitted that the exact position of the transmembrane region varies even between the subunits of *E.coli* hydrogenase; so, one can imagine the possibility of sliding of the transmembrane helix across the membrane bilayer. Hence, the variance between predictions made by TMHMM server could be physiologically negligible.

2.4. Full-size models of the hydrogenases

The presence of long helical moieties in the full-sized small subunits increased their normalized DOPE z-scores significantly, leading to the results that cannot be considered as really good for globular proteins. Since the z-DOPE levels for many enzyme models were above -1 for the small subunits, z-DOPE levels for aligned parts (i.e. parts having the homologous experimentally solved structures) in full-size models were also taken into account.

Nevertheless, one should keep in mind that DOPE statistical potential was developed and calibrated as a scoring function on a sample of cytosolic globular proteins, so the high z-DOPE levels are in agreement with the suggestion of possible role of the C-end fragments as membrane anchors of hydrogenases.

The normalized DOPE z-scores of the aligned parts of the hydrogenase subunits after energy minimization demonstrated values corresponding to high confidence levels. The results of DOPE assessment for hydrogenase subunits are summarized in Supplementary Tables 3 and 4. Analysis of X-ray structure of full-size hydrogenase from E.coli (PDB ID: 4GD3) showed that the structure of its small subunit has quite poor z-DOPE score (-0.476 - -0.513 before energy minimization, -0.547 - -0.619 after), so the results for models and for X-ray structure do not differ much.

Overview of the full-size models of the studied enzymes is shown on Figure 8.

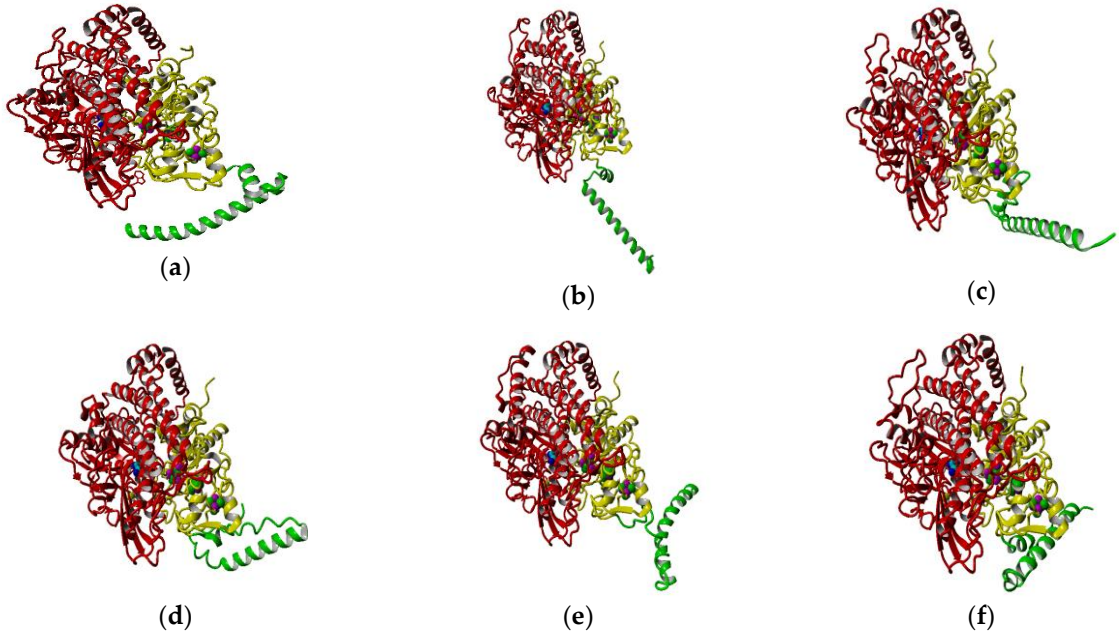

Figure 8. Full-size models of HupSL hydrogenases. Ab initio modeled fragments are coloured green. The panels of the figure correspond to the following enzymes: **(a)** HupSL from *Thiocapsa roseopersicina;* **(b)** HupSL from *Rhodobacter capsulatus*; **(c)** HupSL from *Rhodobacter sphaeroides*; **(d)** HupSL from *Rhodopseudomonas palustris*; **(e)** HupSL from *Rubrivivax gelatinosus*; **(f)** HupSL from *Rhodospirillum rubrum*.

2.5. Intrasubunit and intersubunit interactions

The results of intersubunit interaction assessment showed that the main contributors into the stability of intersubunit interface are hydrophobic contacts; however, there was no statistical significance of the intersubunit interactions in the studied enzymes.

Calculations of hydrogen bonds led to very high dispersions and showed no reliable differences between the enzymes. Other interactions, such as Pi-Pi (aromatic-aromatic), Pi-cationic, aromatic-sulfur, did neither demonstrate reliable differences and made only slight contribution into the overall interaction network of the enzymes. There were three types of interactions that showed statistically significant differences between various enzymes: hydrophobic contacts in the large subunits; ionic pairs in the large subunits; ionic pairs between subunits (Figures 9-11).

It should be noted that models of *Rhodobacter* hydrogenases have significantly lower number of hydrophobic interactions between the residues of large subunits

Preprints (www.preprints.org) | NOT PEER-REVIEWED | Posted: 6 December 2019 doi:10.20944/preprints201912.0083.v1

Peer-reviewed version available at Int. J. Mol. Sci. 2020, 21, 366; doi:10.3390/ijms21010366

(Figure 9). This fact could have an effect onto the stability of enzymes either at elevated temperatures or in presence of solvents other than water. Since large subunit is linked by fewer metal-protein interactions than the small one, its stability could be the limiting factor during denaturation of hydrogenases.

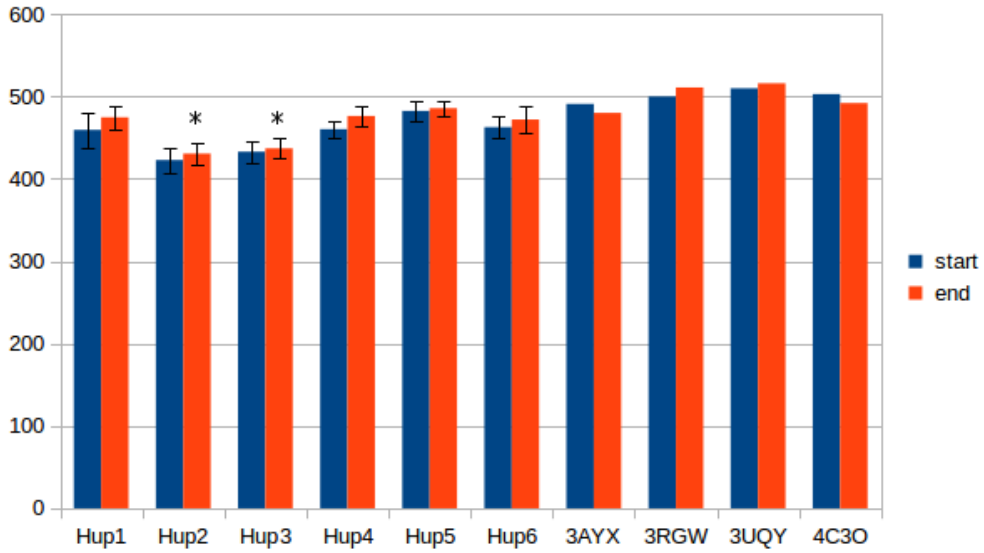

Figure 9. Number of hydrophobic contacts in large subunits of HupSL hydrogenases. **Hup1 -** HupSL from *Thiocapsa roseopersicina;* **Hup2 -** HupSL from *Rhodobacter capsulatus*; **Hup3 -** HupSL from *Rhodobacter sphaeroides*; **Hup4 -** HupSL from *Rhodopseudomonas palustris*; **Hup5 -** HupSL from *Rubrivivax gelatinosus*; **Hup6 -** HupSL from *Rhodospirillum rubrum;* **3AYX -** HoxKG from *Hydrogenovibrio marinus;* **3RGW -** HoxKG from *Ralstonia eutropha;* **3UQY -** HyaAB from *Escherichia coli;* **4C3O -** HydAB from *Salmonella enterica.* Start - models(structures) before energy minimization; end - models(structures) after energy minimization. The data are represented as mean±2*SD. Significantly low results (ranges not overlapping with the others in the subgroup) are marked by asterisk sign.

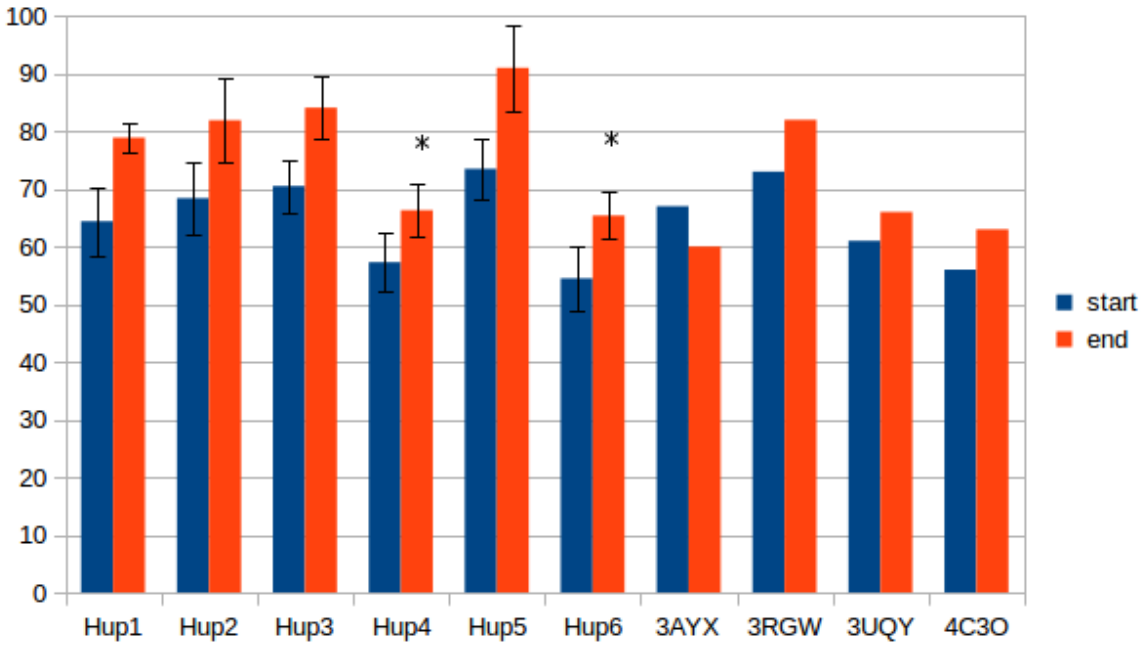

Preprints (www.preprints.org) | NOT PEER-REVIEWED | Posted: 6 December 2019 doi:10.20944/preprints201912.0083.v1

Peer-reviewed version available at Int. J. Mol. Sci. 2020, 21, 366; doi:10.3390/ijms21010366

Figure 10. Number of ionic pairs in large subunits of HupSL hydrogenases. **Hup1 -** HupSL from *Thiocapsa roseopersicina;* **Hup2 -** HupSL from *Rhodobacter capsulatus*; **Hup3 -** HupSL from *Rhodobacter sphaeroides*; **Hup4 -** HupSL from *Rhodopseudomonas palustris*; **Hup5 -** HupSL from *Rubrivivax gelatinosus*; **Hup6 -** HupSL from *Rhodospirillum rubrum;* **3AYX -** HoxKG from *Hydrogenovibrio marinus;* **3RGW -** HoxKG from *Ralstonia eutropha;* **3UQY -** HyaAB from *Escherichia coli;* **4C3O -** HydAB from *Salmonella enterica.* Start - models(structures) before energy minimization; end - models(structures) after energy minimization. The data are represented as mean±2*SD. Significantly low results (ranges not overlapping with the others in the subgroup) are marked by asterisk sign.

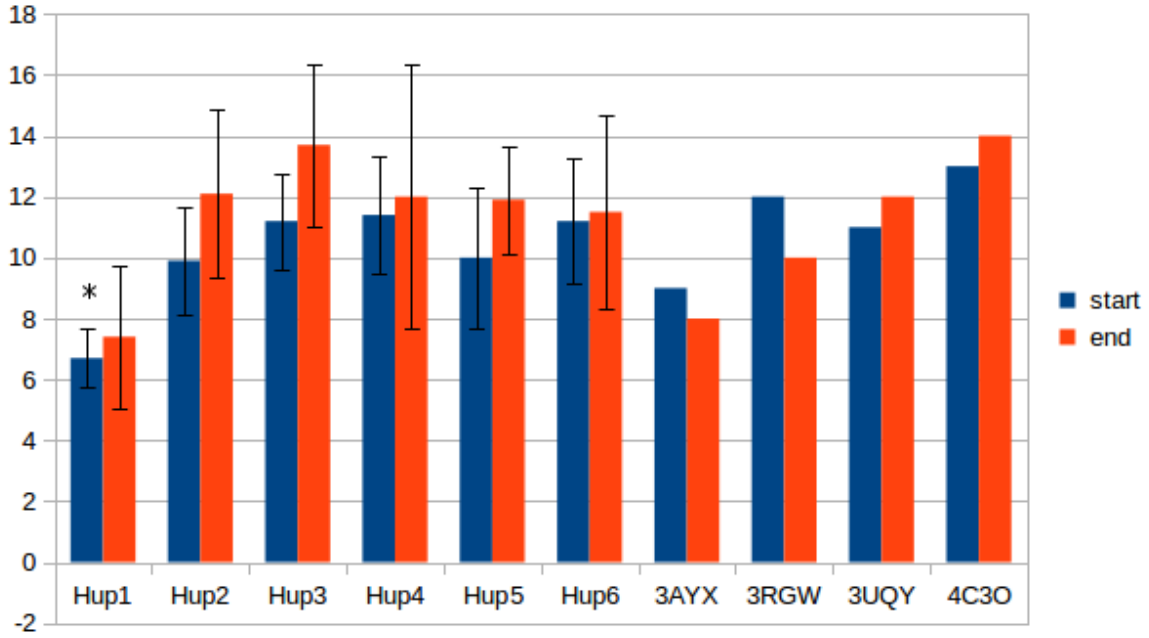

Figure 11. Number of ionic pairs between the subunits of HupSL hydrogenases. **Hup1 -** HupSL from *Thiocapsa roseopersicina;* **Hup2 -** HupSL from *Rhodobacter capsulatus*; **Hup3 -** HupSL from *Rhodobacter sphaeroides*; **Hup4 -** HupSL from *Rhodopseudomonas palustris*; **Hup5 -** HupSL from *Rubrivivax gelatinosus*; **Hup6 -** HupSL from *Rhodospirillum rubrum;* **3AYX -** HoxKG from *Hydrogenovibrio marinus;* **3RGW -** HoxKG from *Ralstonia eutropha;* **3UQY -** HyaAB from *Escherichia coli;* **4C3O -** HydAB from *Salmonella enterica.* Start - models(structures) before energy minimization; end - models(structures) after energy minimization. The data are represented as mean±2*SD. Significantly low results (ranges not overlapping with the others in the subgroup) are marked by asterisk sign.

The results of ionic interaction calculations allow dividing the modeled enzymes into two groups on the basis of number of ionic interactions in their large subunits, "high-ionic" (*T. roseopersicina, R. capsulatus, R. sphaeroides, Rvx. gelatinosus*) and "low-ionic" (*Rsp. rubrum, Rps. palustris*). This statistically significant difference could also affect some properties of the enzymes, for example, thermal stability at different salt concentrations, which could be important when applying these hydrogenases in fuel cells with high ionic strength of the electrolyte. It must be admitted that number of ionic interactions is usually significantly elevated during energy minimization in YASARA force field, as it follows from the results of the present calculations.

As for intersubunit interactions, the low number of ionic pairs in HupSL from *Thiocapsa roseopersicina* admitted by Szilagyi and colleagues [28] was also observed while using models before energy minimization; however, after this procedure, the

distributions of intersubunit ionic pair numbers became wider, so this result apparently lost its statistical significance.

2.6. Molecular tunnels: possible oxygen pathways

The effect of differences of intramolecular tunnel structure on oxygen stability of the studied hydrogenases cannot be considered as definitely significant, because it is not clear what diffusion kinetics would be; however, some differences could be supposed in favor of some of the studied hydrogenases.

Fine tunnel structure depended on energy minimization procedure (whether it was carried out or not). Many tunnels vanished or became more narrow after energy minimization. When starting points were selected between NiFe active site and 4Fe3S-cluster, tunnel structure was very unstable; more stable mapping results were obtained during automatic selection of tunnel structure. There were several tunnels with high hydropathicity level, which could act as gas accession channels. When setting "bottleneck tolerance" parameter to 0 (i.e. all the tunnels with the narrowest point narrower than 1.2 Å were removed), there appeared differences between the studied enzymes (models and X-ray structures from PDB). For instance, only one tunnel close to the active site was mapped in case of HupSL from *Thiocapsa roseopersicina* and HyaAB from *E.coli* (PDB ID: 3UQY) when bottleneck tolerance value was set to zero; two tunnels were mapped in Rhodobacter hydrogenases, but their level of similarity was close to the upper limit (0.7), so they could be treated as one tunnel. Hydrogenase from *Hydrogenovibrio marinus* (PDB ID: 3AYX) showed no tunnels close to the active site in such conditions.

Some of the tunnels start really close to the active site; an example of such a tunnel network is shown below (Figure 12); results of tunnel mapping after automatic starting point selection are given in Supplementary materials.

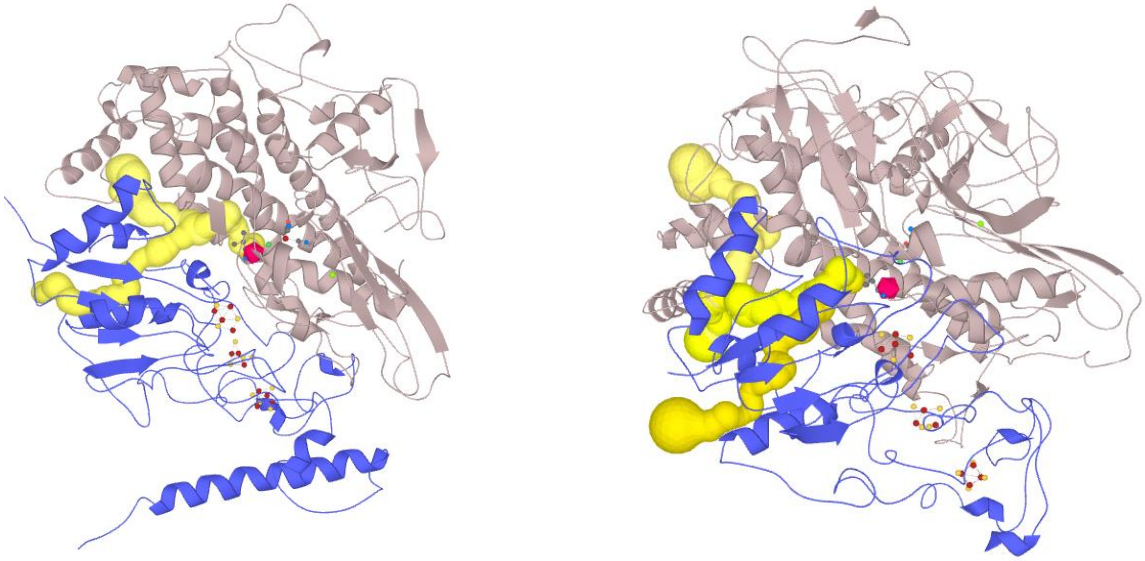

(**a**) (**b**)

Figure 12. Tunnel structure in some of the studied hydrogenases. (a) HupSL from *Rhodospirillum rubrum*; (data available online: https://mole.upol.cz/online/U1IDaUXAtk9G2dt1a54w/1); **(b)** HoxKG hydrogenase from *Ralstonia eutropha* (PDB ID: 3RGW); the most important gas channels (starting in the points close to active site) are coloured yellow(data available

online:https://mole.upol.cz/online/ORQHeeJ90OSUp1FWnBFlg/1); red polyhedron indicates V77, one of the first lining residues of the tunnels close to the active site. Nickel atom is coloured dark-green.

Since tunnel mapping is quite a complicated process dependent on multiple factors, it required verification by comparing with experimental data of Kalms and colleagues [31; 36]. For this purpose, krypton-assessed (PDB ID: 5D51) and oxygen-derived (PDB ID: 5MDL) results of tunnel mapping in *Ralstonia eutropha* membrane-bound hydrogenase were taken. As there are gas molecules present in these PDB files, tunnel-lining residues were calculated by setting a 4 Å distance cutoff from the gas molecules. The detailed results of comparison of hydrogenases from *Rhodospirillum rubrum* and *Ralstonia eutropha* are listed in Supplementary table 7; the level of tunnel similarity allows to make a preliminary conclusion that the tunnel structure is quite similar between two enzymes selected for comparison; the level of tunnel similarity in PDB files of *Ralstonia eutropha* hydrogenase shows some level correlation of mapping with experimental data. Also, lining residues in the modeled enzyme showed a certain level of similarity with the experimental structure. However, it must be admitted that the diversity between the studied hydrogenases does not let to divide them into certain groups to judge about their oxygen tolerance in relation to tunnel structure; other factors, such as the ability to exchange electrons between small subunits in oligomeric state, appear to be more essential in determining oxygen tolerance. Prediction of this ability is described in the next chapter.

2.8. Possible oligomerization: protein-protein docking results

According to data obtained by combined ClusPro docking and PISA assessment of binding energies, mutual binding affinity in the calculated complexes is higher than in reference structure (E. coli hydrogenase, PDB ID: 4GD3). However, it should be admitted that the native E.coli hydrogenase-1 is bound to membrane, and it does also interact with cytochrome molecule; thus, the strong direct interaction between two hydrogenase molecules is not required; as for distances between FeS-clusters of adjacent hydrogenase small subunits in $(HupSL)_2$-heterotetramer, for most cases, they were comparable to those observed in oxygen-tolerant hydrogenase oligomer, but for the enzymes from *Rba. sphaeroides,* the distances were close to 30 Å. This does not mean impossibility of electron transfer, but the role of surrounding aromatic residues as possible "hopping sites" for electrons (intermediate states which could exchange electrons or holes with the FeS clusters) should increase. Figure 13 shows the overview of docking complexes and close view of FeS clusters of two adjacent small subunits in case of two HupSL-HupSL dimers, from *Rba. capsulatus* and *Rba. sphaeroides*.

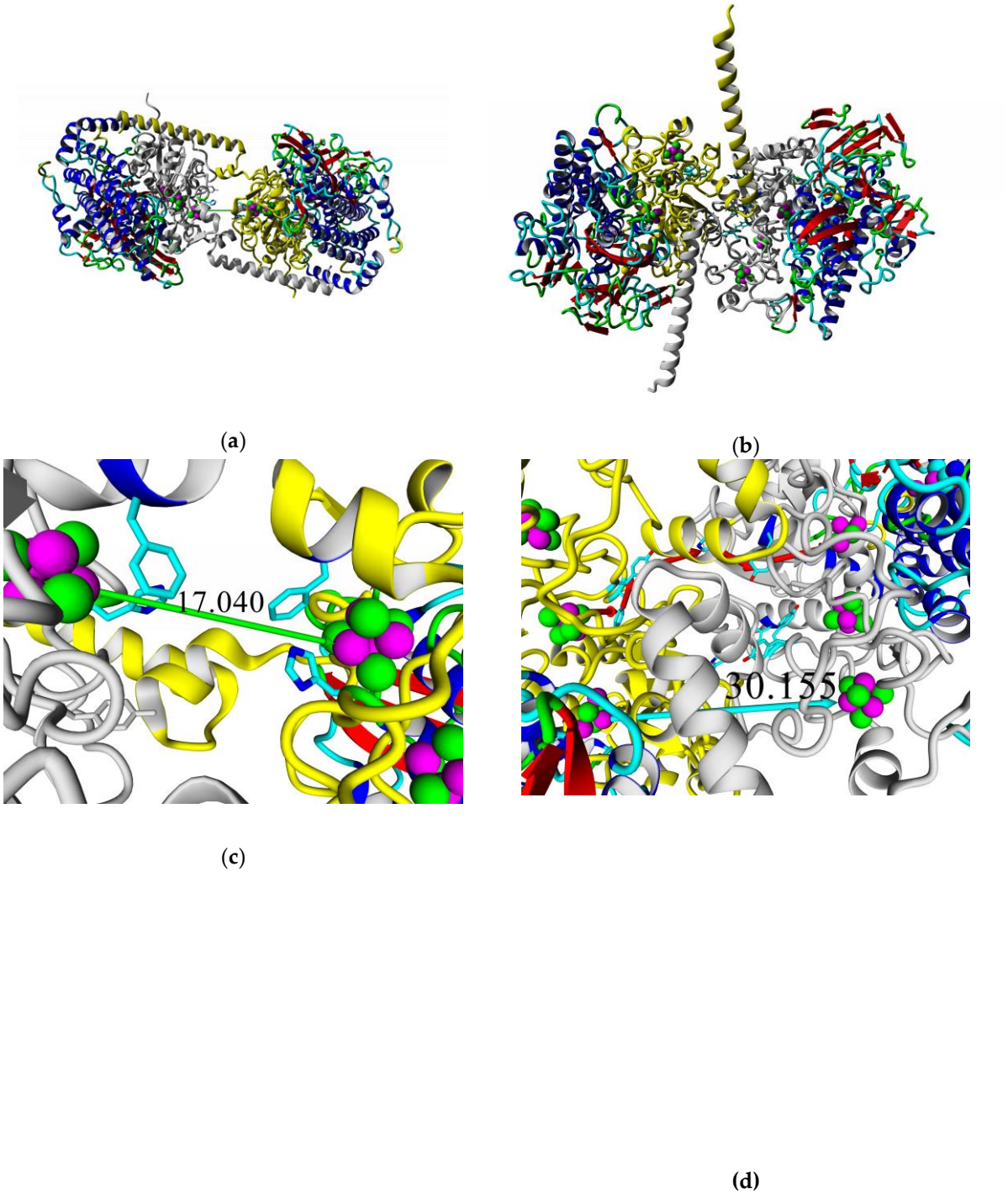

Figure 13. FeS-cluster interaction in HupSL-HupSL hydrogenase oligomers obtained by protein-protein docking. Overview of the oligomers: **(a)** HupSL from *Rhodobacter capsulatus*; **(b)** HupSL from *Rhodobacter sphaeroides.* Small subunits are coloured gray and yellow. Close view of FeS clusters of the adjacent small subunits: **(c)** HupSL from *Rhodobacter capsulatus*; **(d)** HupSL from *Rhodobacter sphaeroides.* Aromatic residues are shown as sticks colored by element coloring scheme. Green and cyan arrows demonstrate the shortest paths of direct electron transfer (distance shown in Å); red arrows **(d)** show possible direction of electron "hopping" throught the network of aromatic residues.

The results of docking-based oligomerization modeling show that the studied enzymes should have the ability to exchange electrons between the FeS clusters of adjacent small subunits, so oxygen tolerance should take place.

2.9. Interaction with electrode compounds: docking of small molecules

The results of molecular docking of conductive compounds showed that the modeled hydrogenases can be promising enough when compared to oxygen-tolerant hydrogenases with resolved X-ray structure. The specificity and affinity of binding in blind docking analysis were comparable to the hydrogenases of hydrogen-oxidizing bacteria (detailed data in Supplementary Tables 9-12).

Thorough analysis of the obtained docking complexes revealed the different modes of binding which could be divided into "productive" and "non-productive" complexes. "Productive" complex means that the distance between FeS clusters and the ligand is less than 20 Å (this is quite an arbitrary value, but in some way it corresponds to the possibility of electron transfer); the ratio of occupancy between these complexes (a fraction of productive complexes) could roughly reflect the probability of binding into productive and non-productive complexes in the real solution (suspension) or on the electrode surface. Moreover, the distance from the closest atom of the ligand to the FeS cluster could serve as a parameter corresponding to electron transfer rate. An example of graphene oxide binding to HupSL from *Rhodobacter sphaeroides* is shown on Figure 14.

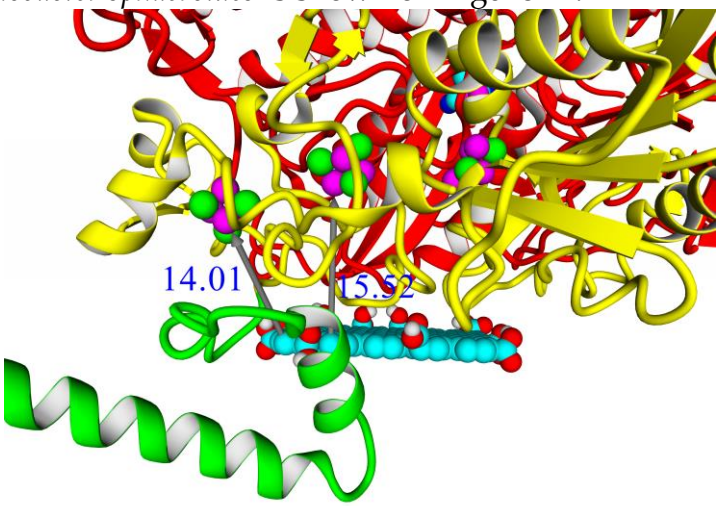

Figure 14. Docking complexes of *Rhodobacter sphaeroides* HupSL hydrogenase and graphene oxide: productive complex. Distances from aromatic plane of graphene oxide are shown by gray arrows and labeled (14.01 Å from the plane to the nearest Fe atom of distal FeS cluster; 15.52 Å from the plane to medial FeS cluster). Colouring scheme as in Figure 4, graphene oxide is coloured by standard YASARA element scheme (carbon - cyan, oxygen - red, hydrogen - gray).

Among all the enzymes assessed by docking, models of HupSL from *Rba. sphaeroides* and *Rvx. gelatinosus* before energy minimization demonstrated the highest fraction of productive complexes with graphene oxide (15/20 and 13/20, respectively - see Supplementary Table 11); after energy minimization in solution, the highest productivity (11/20) was observed for interaction of *Rsp. rubrum* and *H. marinus* hydrogenases with neutral red trimer (Supplementary Table 12).

When comparing the chosen criterion for productivity of the complexes (20 Å distance cutoff), it could seem not strict enough compared to native distances between electron-transferring subunits in hydrogenases or hydrogenase complexes. For example, NiFe-FeS distance is 13.7 Å, the same distance is observed between

distal FeS cluster and heme aromatic group in hydrogenase-1:cytochrome complex of *E.coli* (PDB ID: 4GD3); distances between distal FeS clusters in *S. enterica* hydrogenase oligomer (PDB ID: 4C3O) are also 14 - 16 Å; from the other point of view, there was a work demonstrating that even 32.3 Å distance could be enough for direct electron transfer [37]; however, this was the case of microampere current densities, whereas design of high-current density electrode will require shorter distances from Fe to the surface.

3. Discussion

The HupSL-hydrogenases of purple phototrophic bacteria have been underestimated for quite a long time. Since their discovery in 1950ths-1980ths [38-40], they were considered mostly as something to get rid of in order to improve hydrogen producing strains of purple bacteria (for example, [41]). However, some works did really employ the activities of these enzymes. For example, there were two works on hydrogen production by *Escherichia coli* cultures transformed with Hup-hydrogenase genes from *Rhodobacter sphaeroides* [42] and *Rhodopseudomonas palustris* [43]. Interestingly, both these cases provided significant improvement of hydrogen production by *Escherichia coli*. So, although the catalytic bias of the membrane-bound hydrogenases towards hydrogen oxidation is well-known, and their main physiological role is utilization of hydrogen evolved in nitrogenase reaction [40, 41] but the "uptake" nature of these hydrogenases is not physiologically irreversible.

The aforementioned study of inhibition of HupSL from *Rhodobacter capsulatus* by diphenylene iodonium [27] showed that there should be two binding sites for different electron acceptors; diphenylene iodonium was also demonstrated to inhibit hydrogen production by *Rhodobacter sphaeroides*. The authors suggested that such inhibition was due to interaction of this compound with hydrogenase, rather than with nitrogenase, thus providing extra evidence for HupSL-dependent hydrogen production [44]. Taken together, these data show that the electron flow in HupSL hydrogenases is quite a flexible matter to study, and structural models obtained in the current work would help to understand this complex subject clearer.

A few words must be said about *Rhodospirillum rubrum* hydrogenase. It has been shown to be present preferrably in cultural liquid (overall activity in cultural liquid being 10 times higher than in disrupted cell extracts), and reasonable amounts of the production of this enzyme were achieved by simple addition of EDTA to the cultural medium. This could be explained by its susceptibility to cleavage by a metalloprotease. Adams and Hall demonstrated that this enzyme is deactivated by air (half-life of 7 days in air vs 12 days under N_2 atmosphere) [45]. However, Kakuno et al. showed that this enzyme can be stabilized by EDTA and high salt concentration (no detectable loss of activity in 6 months at salt (NaCl, KCl, CsCl) concentrations above 0.7 M under air; the enzyme tolerated up to 4 M NaCl) [46]. This stabilization cannot be explained just by decrease of oxygen solubility, since it decreases only by 1.5 times. Although the data obtained by Kakuno and colleagues do not evidence that it was exactly Hup-hydrogenase, later data by Manness clarified that among the

three hydrogenase activities two are inducible, and Hup hydrogenase has the highest hydrogen uptaking activity [47]. Low number of ionic pairs shown in the present study for the catalytic subunit of this enzyme could explain its stability towards high salt concentration. So, this makes the *R. rubrum* enzyme a good candidate for experimental assessment in electrochemistry in solutions with high conductivity.

Rubrivivax gelatinosus was studied from the point of view of its ability to catalyze water-gas shift reaction [48]; another study [23] showed that HupSL deletion is an effective way of providing hydrogen production from CO, but nothing could be said about the properties of HupSL hydrogenase.

It should be noted that previous studies did also point onto supernumerary cysteine residues in the small subunits of *Rx. gelatinosus* hydrogenase [49], but this study contained just a remark without detailed examination of the structure of this enzyme. Now, it is time to look at this enzyme as at one of the most promising candidates for the role of novel oxygen-tolerant catalyst (among purple bacteria), since it has the highest similarity of amino acid residues with crystallized oxygen-tolerant enzymes from chemotrophic bacteria. Presence of valine instead of threonine could lead to increased hydropathicity of the region of the 4Fe3S-cluster. Its good binding to graphene oxide (although shown for model before energy minimization) could be its advantage in electrode fabrication; the same can be said about HupSL from *Rhodobacter sphaeroides*.

As for *Thiocapsa roseopersicina*, it is the only sulfur bacteria among all the organisms covered in present modeling study. Its Hup-hydrogenase was not studied as intensely as Hyd- (or Hyn-) hydrogenase. Some studies could lead to proposals that this enzyme is not promising from biotechnological point of view. For example, it was shown to lose its activity irreversibly under air in just a day [26]; since then, it became mostly the subject of basic research exploring regulation of its synthesis [50-51]. But there could arise some interesting information. Several works demonstrated the susceptibility of Hup-hydrogenases towards cold denaturation [38; 50; 52 (p. 83)]. However, the techniques used in these works were not excluding proteolysis (the spectra of used protease inhibitors were insufficient to suppress it completely; moreover, EDTA helped to stabilize the hydrogenase from *Rhodospirillum rubrum*, as was mentioned earlier), so these results should be regarded quite critically. For example, the proteomes of several purple non-sulfur bacteria contain homologs of proteases which are more active in cold environment. These proteases are: DegP-like protein of *R. sphaeroides* 2.4.1 (Uniprot ID: Q3IX80) and *R. capsulatus* SB1003 (Uniprot ID: D5ALS1) both sharing 37% of identical residues with DegP protein from *E. coli* (Uniprot ID: P0C0V0) [53] (comparison was made by the author of the current work); their activities should be investigated thoroughly in cases of preparation of proteins from these bacteria using cold temperature as the simplest way of proteolysis inhibition; perhaps, specific inhibitors of these enzymes should be designed in order to prevent the proteolysis of hydrogenases.

Peer-reviewed version available at Int. J. Mol. Sci. 2020, 21, 366; doi:10.3390/ijms21010366

The number of ionic interactions could presumably be related to proton transfer parameters. If proton transfer could be rate-limiting in certain conditions, the larger number of ionic pairs should correlate with increased hydrogen oxidation/evolution rate. The number of ionic and hydrophobic interactions could be a possible determinant of stability in water or in presence of other solvents, as well as in presence of high electrolyte concentration, but it needs experimental validation.

Rather poor z-DOPE levels of the full-size models of Hup hydrogenases from *Rba. capsulatus, Rba.sphaeroides, Rps.palustris, Rsp. rubrum* can be explained by their hydropathicity and tendency to form membrane anchors, since DOPE statistical potential was calibrated on globular hydrophilic proteins. In other words, quality of the models assessed by z-DOPE somewhat correlated with the results of TMHMM predictions for the presence of transmembrane helices at the C-ends of the studied enzymes. Moreover, the z-DOPE levels are comparable to those shown for hydrogenase-1 from E.coli (PDB ID: 4GD3, 6G94).

Tunnel structure in hydrogenases is quite a complex subject to study, since one should always keep in mind its flexibility. Structure of tunnels in solution could be most accurately reflected by the results on energy-minimized structures; however, when taking into account gaseous electrodes for air-breathing fuel cells, one can suppose that the protein structure and thus tunnel structure could be more accurately approximated by the crystal structure or the frames of *in vacuo* molecular dynamics, since the enzyme is placed in almost dry atmosphere or on hydrophobic surface of carbonaceous material [54]. Nevertheless, the structure of the tunnels mapped in the current work was very diverse, and more reliable results addressing the issue of possible oxygen stability were achieved by protein-protein docking showing that the FeS clusters in oligomers of the modeled enzymes can be close enough to provide intersubunit electron exchange between the small subunits.

When using molecular docking as a method of assessing the prospects of certain redox enzyme in the field of applied electrochemistry, one must take into account the need for formation of a complex that could be formed during the contact of the enzyme with electrode surface. For instance, the plane of graphene oxide must be oriented in such way that it could be expanded to model a plane of carbon; in other case, when the plane is embedded into protein pocket, it could model the behaviour of the enzyme just on the edge of the electrode surface.

The increase of affinity of hydrogenases to neutral red oligomer with the oligomerization degree shows that neutral red dye could also be the promising immobilization agent for these hydrogenases. Since it showed its prospects of application with HydSL hydrogenase from *Thiocapsa roseopersicina* [55], there is definitely a reason to test it in a series of other hydrogenases. In this work, hydrogenase from *Rsp. rubrum*, as well as experimentally resolved *H. marinus* enzyme, showed the highest degree of specificity of neutral red trimer binding.

Beside purely geometrical criteria of hydrogenase sorption efficiency, such as distance from FeS cluster to electrode and angle between the graphene oxide plane and enzyme surface, there is another parameter that was not covered in the current work, namely dipole moment. It was shown to be an important factor of efficient

interaction of membrane-bound hydrogenases from *R. eutropha* [37] and *A. aeolicus* [56] with electrode surfaces; however, the case of high-current density fuel cells seems to require the shortest distance from FeS cluster to electrode surface, dipole moment being the second priority. Moreover, the case of short-range interaction between electrode surface and FeS cluster should increase the impact of local electrostatics of cluster microenvironment, thus decreasing the role of dipole moment of the HupSL dimer as a whole. Nevertheless, dipole moment is definitely an interesting subject for further study.

The biotechnological potential of Hup-hydrogenases should be analyzed not only *in vivo*, but also *in vitro*. Since 4Fe3S-cluster-containing hydrogenases are treated as "oxygen-tolerant", such tolerance should be examined in Hup-hydrogenases from purple bacteria. Despite impressive success of studying *E.coli* and *R.eutropha* hydrogenases achieved so far, there is still no answer on a question which hydrogenase is "the best" for hydrogen fuel cell application, meaning that the whole diversity of probably oxygen-tolerant hydrogenases must be examined in comparative studies and their noticed strengths and weaknesses should lead to creation of the optimal catalyst for future energy.

4. Materials and Methods

Sequences for homology modeling of these enzymes were found in NCBI Protein database. According to modern hydrogenase classification proposed by Sondergaard et al. [32], they were assigned to group 1d of NiFe hydrogenases (Aerobic uptake hydrogenases, oxygen-tolerant, possessing [NiFe]-centre, 1 x [4Fe3S] cluster, 1 x [3Fe4S] cluster, 1 x [4Fe4S] cluster, interacting with b-type cytochrome). The used sequences are listed in table A1 (Appendix A).

Before using the sequences in MODELLER, they were pre-processed based on literature data and multiple alignments. The large subunits were truncated to the last C-terminal histidine residue, since the final step of hydrogenase maturation is cleavage of C-terminal peptide [57]; the sequences of large subunit C-termini are listed in table A2 (Appendix A).

As for the small subunits, the situation was a bit more complicated. Since the small subunit precursors contain twin-arginine motifs, and they were described as being subject to proteolysis accompanying targeting them to periplasm, their N-termini were analyzed to find out the proteolysis sites. The analysis was conducted on three websites, namely SignalP, TatP, LipoP [58-60]. All the three sites did robustly predict cleavage between alanine and methionine or alanine and leucine in the N-terminal part of the small subunits. The signal peptides cleaved off the small subunits and their scores for probabilities of cleavage site presence are listed in Table A3 (Appendix A).

Homology modeling

Homology modeling was carried out in MODELLER program package [28, 61-62]. Templates for homology modeling were searched using BLAST online service

[63], and the alignments produced were taken as the base for writing alignments for using in MODELLER.

Several templates were selected for homology modeling (PDB IDs listed): 3AYX (membrane-bound hydrogenase from *Hydrogenovibrio marinus*), 3RGW (membrane-bound hydrogenase from *Ralstonia eutropha* H16), 3UQY (membrane-bound hydrogenase-1 from *Escherichia coli* K12), 4C3O (*Salmonella typhimurium* LT2); after a series of initial modelling runs, two templates, 3RGW and 3UQY, were kept, whereas other templates were dismissed.

Since Modeller allows multi-subunit modeling, the sequences present in alignments comprised sequences of both large and small subunits of the hydrogenases of interest. The ligands were included into the models as bulk rigid bodies, i.e. they were not recognized by MODELLER as atoms possessing their own forcefield parameters, except Mg which was specially designated by "$" sign and treated like a CHARMM27 atom.

Several strategies implemented into MODELLER were combined to increase the confidence level of homology models: 1) VTFM-optimisation; 2) conjugated gradient optimization; 3) *in vacuo* molecular dynamics. To find the optimal optimization protocol, the optimization procedure was repeated from 1 to 5 times.

The confidence level of the models were assessed via normalized DOPE z-score (z-DOPE) [28] estimation, the values below -1 were considered as very good and reliable according to the recommendation of MODELLER development team. The key value for sorting the models was z-DOPE of a small subunit (aligned part of the subunit only).

Ab initio modeling

QUARK *ab initio* modeling server [64] was used in the work for modeling C-terminal parts of the small subunits of these enzymes. The data obtained from these servers were collected and ranked by the server itself based on their TM-score; they were used as templates for building 100 models in MODELLER with optimization by high-temperature molecular dynamics *in vacuo* and the best models assessed by normalized DOPE z-score were used for the following MD simulation in water.

Molecular dynamics simulation

To improve the quality of *ab initio* predicted models of C-terminal parts of the small subunits, molecular dynamics simulations in explicit water during 20 ns were performed in GROMACS [65]. The initial files for molecular dynamics in GROMACS were produced from MODELLER calculations, where the results from QUARK web server were used as templates for the homology modeling calculations, and the final models were selected based on their lowest z-DOPE scores from 100 models of the fragments.

For better concordance of MODELLER and GROMACS simulations, CHARMM22 force field [66] was selected for all the steps of molecular dynamics in GROMACS.

The boundaries for all the simulations were periodic.

Energy minimization was performed by steepest descent algorithm until the maximum force was less than 1000kJ/mol/nm. Long-range electrostatic interactions were calculated by Particle Mesh Ewald (PME) method; short-range electrostatic and Van-der-Waals cut-off radii were 1 nm; spc water model was used for solvation of the protein in a cubic box extended by 1 nm from the protein; 100ps NVT (in modified Berendsen thermostat [67]) and NPT (in modified Parrinello-Raman barostat [68]) calculations were followed by 20ns production molecular dynamics.

The resulting frames were saved every 4 ns, so that 5 conformers of C-terminal part of the small subunits were used in modeling the full HupSL dimers.

Assessment of the role of ab initio modeled parts in membrane anchoring

To predict the tendency of the studied fragments to form transmembrane alpha-helices, they were analyzed on TMHMM server, version 2.0 [30] (*www.cbs.dtu.dk/services/TMHMM/*).

Full-size hydrogenase modeling

Full-size hydrogenase modeling was carried out in MODELLER using the alignments expanded by addition of C-terminal fragments to modeled hydrogenase sequences; the conformers of C-terminal domains obtained from molecular dynamics in explicit water were assessed by normalized DOPE z-score and those having the lowest values were used as templates for C-terminal parts. The optimization scheme was the same as before, i.e. VTFM-optimization and high-temperature molecular dynamics *in vacuo*.

Intrasubunit and intersubunit interaction assessment

Intra- and intersubunit interactions were estimated on Protein Interaction Calculator Web server (http://pic.mbu.iisc.ernet.in/) [69].

Electrostatic interactions were assessed by the same criterion as in the work (Szilagyi et al. 2002): the cutoff for centroid-centroid distance was set to 6 Å [25].

Hydrophobic contacts were counted as number of atom-atom distances less than 5 Å between aliphatic or aromatic carbons of the following residues: Ala, Val, Leu, Ile, Met, Phe, Trp, Pro, Tyr.

Aromatic-aromatic interactions were calculated as number of distances in range from 4.5 to 7 Å between aromatic group centroids.

Intramolecular tunnels

To find out possible pathways for gas diffusion inside the studied hydrogenases, intramolecular tunnels were mapped on MOLE2.5 server (mole.upol.cz) [70]. First, NiFe active site was used as starting point for the tunnels; automatic selection of starting point was chosen in further calculations. Hydrogen atoms were ignored, whereas HETATM groups were taken into account. All the other settings were taken by default: origin radius 5 Å, surface cover radius 10 Å, bottleneck radius 1.2 Å, bottleneck tolerance 3 (changed to 0 in the second round of mapping), maximal

tunnel similarity 0.7. Tunnel mapping was performed in both non-minimized and minimized models of Hup-hydrogenases and compared with X-ray structures of hydrogenases from *Hydrogenovibrio marinus* (3AYX), *Ralstonia eutropha* (3RGW), *Escherichia coli* (3UQY), *Salmonella enterica* (4C3O).

Protein-protein docking and oligomerization assessment

The obtained models (HupSL-dimers) were submitted to ClusPro web server [71]. After obtaining the results, they were analyzed on PISA web server [72]; oligomeric structure of Escherichia coli hydrogenase (PDB ID: 4GD3) was taken as reference enzyme. The best ClusPro variants were superposed with the initially submitted models to extract heteroatomic groups in correct positions. Distances between FeS-clusters were measured as the shortest distances between Fe atoms. Aromatic residues between the Fe atoms of adjacent small subunits were regarded as "hopping points" for electron.

Docking of small molecules

Hydrogenase models were prepared for docking in Autodock Tools [73-74]. Polar hydrogens were added, Kollman charges were calculated and AD4 atom types were assigned during receptor preparation. The following ligands were used in docking study: neutral red monomer, dimer and trimer, and graphene oxide as a model of carbon electrode surface. Oligomers of neutral red were modeled acccording to Paulikaite et al. [75]; graphene oxide molecule was taken from PubChem (PubChem CID:124202900) and converted into 3D PDB file in Corina (https://www.mn-am.com/online_demos/corina_demo) [76]. Docking was performed in Autodock Vina [73]. Box size for docking was 120*120*120 Å; number of complexes was set to 20, and exhaustiveness parameter was set to 100 (for the case of graphene oxide, everything looked similar to the approach used by Sumaryada et al. [77].

5. Conclusions

To summarize the results covered by the present article, the author should highlight several important conclusions drawn from the work. First of all, presence of 4Fe-3S cluster was confirmed by homology modeling of spatial structure in six hydrogenases from purple bacteria. Moreover, these hydrogenases were shown to be able to oligomerize in complexes providing electron exchange between adjacent small subunits. Next, the heterogeneity of the cluster's microenvironment was shown; the hydrogenase from *Rubrivivax gelatinosus* was shown to be very alike to common membrane-bound oxygen-tolerant hydrogenases. Third, the C-ends of the small subunits were assessed as possible membrane anchors and motifs of potential oligomerization. Fourth, analysis of large amount of data gave statistically significant differences between the number of hydrophobic and ionic interactions in the studied enzymes. Fifth, molecular docking studies showed basically the same results for the studied enzymes and for the X-ray structures, with a slight advantage of HupSL enzymes from *Rba. sphaeroides* and *Rvx.gelatinosus* in case of graphene oxide and *Rsp.rubrum* in case of neutral red trimer.

Peer-reviewed version available at *Int. J. Mol. Sci.* **2020**, *21*, 366; doi:10.3390/ijms21010366

Supporting information is available in the following files:

.zip archive of the built models (10 models for each studied enzyme) and .xls table of protein-protein interactions from PIC web server;

.zip archive of molecular docking results for graphene oxide and neutral red dye;

.zip archive of the tunnels mapped in the work (data from MOLE2.5 server);

.zip archive of the tunnels mapped in the work with zero bottleneck tolerance (data from MOLE2.5 server);

.html file of transmembrane helix mapping;

.doc files describing the details of supporting information and listing the computational resources

Supplementary tables.

Funding:

This research was funded by Russian Ministry of Science and Education (AAAA-A17-117030110141-2). Article processing charge was paid from personal savings of the author.

Acknowledgments: The author would like to express his gratitude to all the authors and caretakers of the programs and web services used in the work, especially YASARA, Protein Interaction Calculator, MODELLER, QUARK, Mole2.5, ClusPro, PISA, Autodock VINA; beside that, the author thanks Konstantin Alexandrovich Isaev, system administrator of IBBP RAS, for his honorable labour providing the opportunity to work; and, the last but not the least, special thanks to Tony Sumaryada and his colleagues, who inspired to use large molecule in docking in Autodock VINA and expanded the horizons of docking applicability by their brave work.

Conflicts of Interest: The author declares no conflict of interest. The funders (except the author) had no role in the design of the study; in the collection, analyses, or interpretation of data; in the writing of the manuscript, or in the decision to publish the results

Abbreviations

MD	Molecular dynamics
PDB	Protein Data Bank
DOPE	discrete optimized protein energy

Appendix A

Tables of sequences used in the work.

Table 1. The sequences of hydrogenase subunits used in modeling.

Organism (strain)	Large subunit ID	Small subunit ID
Thiocapsa roseopersicina BBS	AAA27410.1	AAA27409.1
Rhodobacter capsulatus (Multistrain)	WP_013066512.1	WP_013066511.1
Rhodobacter sphaeroides WS8N	WP_002720659.1	WP_002720658.1
Rhodopseudomonas palustris CGA009	WP_011156496.1	WP_011156495.1
Rubrivivax gelatinosus IL144	WP_014429772.1	BAL96914.1
Rhodospirillum rubrum F11 (S1)	WP_011388917.1	WP_011388916.1

Table 2. Lists of C-terminal sequences of the large subunits of hydrogenases. Four residues comprising the C-end of mature large subunits are shown in bold type; the residues removed by proteolytic cleavage are shown in italic ; the sites of proteolysis are marked by single quotation marks.

Organism (strain)	Large subunit ID	Large subunit C-terminus
Thiocapsa roseopersicina BBS	AAA27410.1	**CATH'** *IMGPDGEELTRIKVR*
Rhodobacter capsulatus (Multistrain)	WP_013066512.1	**CSTH'** *VMSAEGAPLTTVKVR*
Rhodobacter sphaeroides WS8N	WP_002720659.1	**CSTH'** *VLSPDGQELTTVKVR*

Rhodopseudomonas palustris CGA009	WP_011156496.1	**CSTH'** *VMSEDGQEMAQVKVS*
Rubrivivax gelatinosus IL144	WP_014429772.1	**CSTH'** *VMSEDGRELTTVKVR*
Rhodospirillum rubrum F11 (S1)	WP_011388917.1	**CSTH'** *ILTPEGGEAISVTVR*

International Journal of
Molecular Sciences

Table 3. Lists of sequences removed from the small subunits of hydrogenases before 3d structure modeling. Six residues comprising the N-end of mature small subunit are shown in bold type. For *Rubrivivax gelatinosus*, the row is highlighted in red because of low SignalP5.0 score; higher score predicting reliable cleavage of TAT peptide was observed when starting from the second methionine residue.

Organism (strain)	Small subunit ID	Small subunit N-terminal sequence; SignalP5.0 score
Thiocapsa roseopersicina BBS	AAA27409.1	MPTTETYYEVMRRQGITRRSFLKFCSLTATALGLSPTFAGKIAHA**METKPR** **SignalP5.0 score: 0.8429**
Rhodobacter capsulatus (Multistrain)	WP_013066511.1	MSDIETFYDVMRRQGITRRSFMKFCSLTAAALGLGPSFVPKIAEA**METKPR** **SignalP5.0 score: 0.9668**
Rhodobacter sphaeroides WS8N	WP_002720658.1	-MPQIETFYDVMRRQGITRRSFMKYCSLTAAALGLGPSFVPKIAHA**METKPR** **SignalP5.0 score: 0.9696**
Rhodopseudomonas palustris CGA009	WP_011156495.1	----------MGAVTETFYEVIRRQGITRRSFVKFCSLTATSLGLGPIGATQIAHA**LETKPR** **SignalP5.0 score: 0.9319**
Rubrivivax gelatinosus IL144	BAL96914.1	MTWNGRSGVSLDQGKAGTHRGCELGQRPNPREEPDPMETFYEVMRRQGISRRSFLKYCSLTATSLGLAPSFVPQIAHA**METKPR** **SignalP5.0 score: 0.21 (0.9817 when starting from the second methionine residue)**
Rhodospirillum rubrum F11 (S1)	WP_011388916.1	MGETETFYEVIRRQGISRRGFLKFCGVTAAGLGLGAGGAARIAQA**LETKPR** **SignalP5.0 score: 0.9546**

International Journal of
Molecular Sciences

References

1. Wang G.S.; Grammel H.; Abou-Aisha K.; Sägesser R.; Ghosh R. High-level production of the industrial product lycopene by the photosynthetic bacterium Rhodospirillum rubrum. *Appl Environ Microbiol* **2012** , *20*, 7205-7215
2. Urakami T.; Yoshida T. Production of ubiquinone and bacteriochlorophyll a by Rhodobacter sphaeroides and Rhodobacter sulfidophilus. *Journal of Fermentation and Bioengineering* **1993,** *76 (3),* 191-194
3. Ranaivoarisoa T.O.; Singh R.; Rengasamy K.; Guzman M.S.; Bose A. Towards sustainable bioplastic production using the photoautotrophic bacterium Rhodopseudomonas palustris TIE-1. *J Ind Microbiol Biotechnol* **2019** Mar 29. doi: 10.1007/s10295-019-02165-7. [Epub ahead of print]
4. Koh R.H.; Song H.G. Effects of application of Rhodopseudomonas sp. on seed germination and growth of tomato under axenic conditions. *J Microbiol Biotechnol* **2007,** *17(11),* 1805-1810
5. Schön G; Biedermann M. Growth and adaptive hydrogen production of Rhodospirillum rubrum (F 1) in anaerobic dark cultures. *Biochim Biophys Acta* **1973,** *304(1)*: 65-75
6. Sigma-Aldrich website. Available online. URL: https://www.sigmaaldrich.com/catalog/product/roche/3hbdbro?lang=en&region=RU (Accessed on 28.08.2019)
7. Stephenson M.; Stickland L.H. Hydrogenase: a bacterial enzyme activating molecular hydrogen: The properties of the enzyme. *Biochem J* **1931,** *25(1),* 205-214
8. Pershad H.R.; Duff J.L.; Heering H.A.; Duin E.C.; Albracht S.P.; Armstrong F.A. Catalytic electron transport in Chromatium vinosum [NiFe]-hydrogenase: application of voltammetry in detecting redox-active centers and establishing that hydrogen oxidation is very fast even at potentials close to the reversible H+/H2 value. *Biochemistry* **1999,** *38(28),* 8992-8999
9. Yaropolov A.I.; Karyakin A.A.; Varfolomeev S.D.; Berezin I.V. Mechanism of H2-electrooxidation with immobilized hydrogenase. *Bioelectrochemistry and Bioenergetics* **1984,** *3-4*, 267-277
10. Jones A.K.; Sillery E.; Albracht S.P; Armstrong F.A. Direct comparison of the electrocatalytic oxidation of hydrogen by an enzyme and a platinum catalyst. *Chem Commun (Camb)* **2002,** *8*, 866-867
11. Morozov S.V.; Karyakina E.E.; Zorin N.A.; Varfolomeyev S.D.; Cosnier S.; Karyakin A.A. Direct and electrically wired bioelectrocatalysis by hydrogenase from Thiocapsa roseopersicina. *Bioelectrochemistry* **2002,** *55(1-2),* 169-171
12. Shastik E.S.; Vokhmyanina D.V.; Zorin N.A.; Voronin O.G.; Karyakin A.A; Tsygankov A.A. Demonstration of hydrogenase electrode operation in a bioreactor // *Enzyme Microb Technol* **2011,** *49,* 453–458
13. Shomura Y., Yoon K.S., Nishihara H., Higuchi Y. Structural basis for a [4Fe-3S] cluster in the oxygen-tolerant membrane-bound [NiFe]-hydrogenase. *Nature* **2011,** *479,* 253–256
14. Fritsch J.; Scheerer P.; Frielingsdorf S.; Kroschinsky S.; Friedrich B.; Lenz O.; Spahn C.M. The crystal structure of an oxygen-tolerant hydrogenase uncovers a novel iron-sulphur centre. *Nature* **2011,** *479(7372),* 249-252
15. Volbeda A.; Amara P.; Darnault C.; Mouesca J.M.; Parkin A.; Roessler M.M.; Armstrong F.A.; Fontecilla-Camps J.C. X-ray crystallographic and computational studies of the O2-tolerant [NiFe]-hydrogenase 1 from Escherichia coli. *Proc Natl Acad Sci USA* **2012,** *109(14),* 5305-5310
16. Bowman L.; Flanagan L.; Fyfe P.K.; Parkin A.; Hunter W.N.; Sargent F. How the structure of the large subunit controls function in an oxygen-tolerant [NiFe]-hydrogenase. *Biochem J* **2014,** *458(3),* 449-458
17. Vignais P.M.; Dimon B.; Zorin N.A.; Tomiyama M.; Colbeau A. Characterization of the hydrogen-deuterium exchange activities of the energy-transducing HupSL hydrogenase and H(2)-signaling HupUV hydrogenase in Rhodobacter capsulatus. *J Bacteriol* **2000,** *182(21)* 5997-6004
18. Duché O.; Elsen S.; Cournac L.; Colbeau A. Enlarging the gas access channel to the active site renders the regulatory hydrogenase HupUV of Rhodobacter capsulatus O2 sensitive without affecting its transductory activity. *FEBS J* **2005,** *272(15),* 3899-3908
19. Maroti J. Metabolic versatility of [NiFe]-hydrogenases in *Thiocapsa roseopersicina*. PhD thesis. Hungary. 2010.

20. Xu H.W.; Love J.; Borghese R.; Wall J.D. Identification and isolation of genes essential for H2 oxidation in Rhodobacter capsulatus. *J Bacteriol* **1989,** *171(2),* 714-721
21. Lee I.H.; Park J.Y.; Kho D.H.; Kim M.S.; Lee J.K. Reductive effect of H(2) uptake and poly-beta-hydroxybutyrate formation on nitrogenase-mediated H(2) accumulation of Rhodobacter sphaeroides according to light intensity. *Appl Microbiol Biotechnol* **2002,** *60(1-2),* 147-153
22. Rey F.E.; Oda Y.; Harwood C.S. Regulation of uptake hydrogenase and effects of hydrogen utilization on gene expression in Rhodopseudomonas palustris. *J Bacteriol* **2006,** *188(17),* 6143-6152
23. Sato T.; Inoue K.; Sakurai H.; Nagashima K.V.P. Effects of the deletion of hup genes encoding the uptake hydrogenase on the activity of hydrogen production in the purple photosynthetic bacterium Rubrivivax gelatinosus IL144. *J Gen Appl Microbiol* **2017,** *63(5),* 274-279
24. Kern M.; Klipp W.; Klemme J.H. Increased Nitrogenase-Dependent H(2) Photoproduction by hup Mutants of Rhodospirillum rubrum. *Appl Environ Microbiol* **1994** *60(6)* 1768-1774
25. Szilagyi A.; Kovacs K.L.; Rakhely G.; Zavodszky P. Homology modeling reveals the structural background of the striking difference in thermal stability between two related [NiFe] hydrogenases. *J Mol Model* **2002,** *8*, 58–64
26. Rakhely G.; Colbeau A.; Garin J.; Vignais P.M.; Kovacs K.L. Unusual organization of the genes coding for HydSL, the stable [NiFe]hydrogenase in the photosynthetic bacterium Thiocapsa roseopersicina BBS. *J Bacteriol* **1998,** *180(6),* 1460-1465
27. Magnani P.; Doussiere J.; Lissolo T. Diphenylene iodonium as an inhibitor for the hydrogenase complex of Rhodobacter capsulatus. Evidence for two distinct electron donor sites. Biochim Biophys Acta 2000, 1459(1), 169-178
28. Shen M., Sali A. Statistical potential for assessment and prediction of protein structures. *Protein Sci* **2006,** *15,* 2507–2524
29. Krieger E.; Dunbrack R.L. Jr.; Hooft R.W.; Krieger B. Assignment of protonation states in proteins and ligands: combining pKa prediction with hydrogen bonding network optimization. *Methods Mol Biol* **2012.,** *819,* 405–421
30. Krieger E.; Joo K.; Lee J.; Lee J.; Raman S.; Thompson J.; Tyka M.; Baker D.; Karplus K. Improving physical realism, stereochemistry, and side-chain accuracy in homology modeling: four approaches that performed well in CASP8. *Proteins* **2009,** *77,* 114–122
31. Kalms J.; Schmidt A.; Frielingsdorf S.; Utesch T.; Gotthard G.; von Stetten D.; van der Linden P.; Royant A.; Mroginski M.A.; Carpentier P.; Lenz O.; Scheerer P. Tracking the route of molecular oxygen in O2-tolerant membrane-bound [NiFe] hydrogenase. *Proc Natl Acad Sci USA* **2018**, *115(10),* E2229-E2237
32. Søndergaard D.; Pedersen C.N.; Greening C. HydDB: A web tool for hydrogenase classification and analysis. *Sci Rep* **2016,** *6*, 34212
33. Krogh A.; Larsson B.; von Heijne G.; Sonnhammer E.L.L. Predicting transmembrane protein topology with a hidden Markov model: Application to complete genomes. *Journal of Molecular Biology* **2001,** *305(3),* 567-580
34. Volbeda A.; Darnault C.; Parkin A.; Sargent F.; Armstrong F.A.; Fontecilla-Camps J.C. Crystal structure of the O(2)-tolerant membrane-bound hydrogenase 1 from Escherichia coli in complex with its cognate cytochrome b. *Structure* **2013,** *21(1),* 184-190
35. Volbeda A.; Mouesca J.M.; Darnault C.; Roessler M.M.; Parkin A.; Armstrong, F.A.; Fontecilla-Camps, J.C. X-ray structural, functional and computational studies of the O2-sensitive E. coli hydrogenase-1 C19G variant reveal an unusual [4Fe-4S] cluster. *Chem Commun (Camb)* **2018**, *54,* 7175-7178
36. Kalms J.; Schmidt A.; Frielingsdorf S.; van der Linden P.; von Stetten D.; Lenz O.; Carpentier P.; Scheerer P. Krypton Derivatization of an O2 -Tolerant Membrane-Bound [NiFe] Hydrogenase Reveals a Hydrophobic Tunnel Network for Gas Transport. *Angew Chem Int Ed Engl* **2016,** 55(18), 5586-5590
37. Heidary N.; Utesch T.; Zerball M.; Horch M.; Millo D.; Fritsch J.; Lenz O.; von Klitzing R.; Hildebrandt P.; Fischer A.; Mroginski M.A.; Zebger I.et al. Orientation-Controlled Electrocatalytic Efficiency of an Adsorbed Oxygen-Tolerant Hydrogenase. *PLoS ONE* **2015,** *10(11),* e0143101
38. Gest H. Properties of cell-free hydrogenases of Escherichia coli and Rhodospirillum rubrum. *J Bacteriol* **1952,** *63(1),* 111-121
39. Krasna A.I.; Rittenberg D. A comparison of the hydrogenase activities of different microorganisms. *Proc Natl Acad Sci USA* **1956,** *42(4),* 180-185
40. Gogotov I.N. Hydrogenases of phototrophic microorganisms. *Biochimie* **1986,** *68(1),* 181-187

41. Liang Y.; Wu X.; Gan L.; Xu H.; Hu Z.; Long M. Increased biological hydrogen production by deletion of hydrogen-uptake system in photosynthetic bacteria. *Microbiol Res* **2009,** *164,* 674–679
42. Lee S.Y.; Lee H.J.; Park J.-M.; , Lee J.H.; Park J.-S.; Shin H.S.; Kim Y.-H.; Min J. Bacterial hydrogen production in recombinant Escherichia coli harboring a HupSL hydrogenase isolated from Rhodobacter sphaeroides under anaerobic dark culture. *Int J Hydrog Energy* **2010,** *35(3),* 1112-1116
43. Zhou P.; Wang Y.; Gao R.; Tong J.; Yang Z. Transferring [NiFe] hydrogenase gene from Rhodopeseudomonas palustris into E. coli BL21(DE3) for improving hydrogen production. *Int J Hydrog Energy* **2015**, *40(12),* 4329-4336
44. Hakobyan L.; Gabrielyan L.; Trchounian A. Relationship of proton motive force and the F(0)F (1)-ATPase with bio-hydrogen production activity of Rhodobacter sphaeroides: effects of diphenylene iodonium, hydrogenase inhibitor, and its solvent dimethylsulphoxide. *J Bioenerg Biomembr* **2012,** *44(4),* 495-502
45. Adams M.W.; Hall D.O. Properties of the solubilized membrane-bound hydrogenase from the photosynthetic bacterium Rhodospirillum rubrum. *Arch Biochem Biophys* **1979,** *195(2),* 288-299
46. Kakuno T.; Hiura H.; Yamashita J.; Bartsch R.G.; Horio T. Complete stabilization of water-soluble hydrogenase from Rhodospirillum rubrum under air atmosphere with a high concentration of chloride ions. *J Biochem* **1978,** *84(6),* 1649-1651
47. Maness P.C.; Weaver P.F. Evidence for three distinct hydrogenase activities in Rhodospirillum rubrum. *Appl Microbiol Biotechnol* **2001,** *57(5-6),* 751-756
48. Maness P.C.; Smolinski S.; Dillon A.C.; Heben M.J.; Weaver P.F. Characterization of the oxygen tolerance of a hydrogenase linked to a carbon monoxide oxidation pathway in Rubrivivax gelatinosus. *Appl Environ Microbiol* **2002,** *68(6),* 2633-2636
49. Wawrousek K.; Noble S.; Korlach J.; Chen J.; Eckert C.; Yu J.; Maness P.C. Genome annotation provides insight into carbon monoxide and hydrogen metabolism in Rubrivivax gelatinosus. *PLoS One* **2014,** *9(12),* e114551
50. Palágyi-Mészáros L.S.; Maróti J.; Latinovics D.; Balogh T.; Klement E.; Medzihradszky K.F.; Rákhely G.; Kovács K.L. Electron-transfer subunits of the NiFe hydrogenases in Thiocapsa roseopersicina BBS. *FEBS J* **2009,** *276(1),* 164-174
51. Nagy I.K.; Kovács K.L.; Rákhely G.; Maróti G. HupO, a Novel Regulator Involved in Thiosulfate-Responsive Control of HupSL [NiFe]-Hydrogenase Synthesis in Thiocapsa roseopersicina. *Appl Environ Microbiol,* **2016,** *82(7),* 2039–2049
52. Serebryakova L.T. Hydrogenases of phototrophic organisms. PhD thesis. USSR. 1990. [Material in Russian]
53. The UniProt Consortium. UniProt: a hub for protein information. *Nucleic Acids Res* **2015,** *43*, D204–D212
54. Matsumoto T.; Eguchi S.; Nakai H.; Hibino T.; Yoon K.S.; Ogo S. [NiFe]Hydrogenase from Citrobacter sp. S-77 surpasses platinum as an electrode for H2 oxidation reaction. *Angew Chem Int Ed Engl* **2014,** *53(34),* 8895-8898
55. Voronin O.G.; Konischeva E.V.; Zorin N.A.; Fedotenkov F.A.; Karyakina E.E.; Karpachova G.P.; Orlov A.V.; Kiseleva S.G.; Karyakin A.A. Modification of the electrode surface with analogues of hydrogenase substrates for highly active fuel bioelectrocatalysts development, *Nano-Microsystems Techn*, **2013,** *5*, 15–19
56. Oteri F.; Ciaccafava A.; de Poulpiquet A.; Baaden M.; Lojou E.; Sacquin-Mora S. The weak, fluctuating, dipole moment of membrane-bound hydrogenase from Aquifex aeolicus accounts for its adaptability to charged electrodes. *Phys Chem Chem Phys,* **2014,** *16(23),* 11318-11322
57. Senger M.; Stripp S.T.; Soboh B. Proteolytic cleavage orchestrates cofactor insertion and protein assembly in [NiFe]-hydrogenase biosynthesis. *J Biol Chem* **2017,** *292(28),* 11670-11681
58. Almagro Armenteros J.J.; Tsirigos K.D.; Sønderby C.K.; Petersen T.N.; Winther O.; Brunak S.; von Heijne G.; Nielsen H. SignalP 5.0 improves signal peptide predictions using deep neural networks. *Nat Biotechnol* **2019,** *37(4),* 420-423
59. Bendtsen J.D.; Nielsen H.; Widdick D.; Palmer T.; Brunak S. Prediction of twin-arginine signal peptides. *BMC Bioinformatics* **2005,** *6,* 167

60. Rahman O.; Cummings S.P.; Harrington D.J.; Sutcliffe I.C. Methods for the bioinformatic identification of bacterial lipoproteins encoded in the genomes of Gram-positive bacteria. *World J Microbiol Biotechnol* **2008,** *24(11),* 2377-2382
61. Sali A.; Blundell T.L. Comparative protein modelling by satisfaction of spatial restraints. *J Mol Biol* **1993,** *234,* 779–815
62. Webb B.; Sali A. Comparative Protein Structure Modeling Using Modeller. In *Current Protocols in Bioinformatics* John Wiley & Sons, Inc., Vol. 54, 5.6.1-5.6.37, 2016.
63. Altschul S.F.; Gish W.; Miller W.; Myers E.W.; Lipman D.J. Basic local alignment search tool *J Mol Biol* **1990,** *215,* 403–410
64. Xu D.; Zhang Y. Ab initio protein structure assembly using continuous structure fragments and optimized knowledge-based force field. *Proteins* **2012,** *80,* 1715–1735
65. Abraham M.; Murtola T.; Schulz R.; Páll S.; Smith J.; Hess B.; Lindahl E. GROMACS: High performance molecular simulations through multi-level parallelism from laptops to supercomputers. *SoftwareX* **2015,** *1-2,* 19-25
66. MacKerell A.D.; Bashford D.; Bellott M.; Dunbrack R.L.; Evanseck J.D.; Field M.J.; Fischer S.; Gao J.; Guo H.; Ha S.; Joseph-McCarthy D.; Kuchnir L.; Kuczera K.; Lau F.T.; Mattos C.; Michnick S.; Ngo T.; Nguyen D.T.; Prodhom B.; Reiher W.E.; Roux B.; Schlenkrich M.; Smith J.C.; Stote R.; Straub J.; Watanabe M.; Wiórkiewicz-Kuczera J.; Yin D.; Karplus M. All-atom empirical potential for molecular modeling and dynamics studies of proteins. *J Phys Chem B* **1998,** *102(18),* 3586-3616
67. Berendsen H.J.C.; van der Spoel D.; van Drunen R. GROMACS: A message-passing parallel molecular dynamics implementation. *Comp Phys Comm* **1995,** *91(1–3),* 43-56
68. Parrinello M.; Rahman A. Polymorphic transitions in single crystals: A new molecular dynamics method. *J Appl Phys*, **1981,** *52,* 7182
69. Tina K.G.; Bhadra R.; Srinivasan N. PIC: Protein Interactions Calculator. *Nucleic Acids Res* **2007**, *35,* W473–W476
70. Pravda L.; Sehnal D.; Toušek D.; Navrátilová V.; Bazgier V.; Berka K.; Svobodová Vařeková R.; Koča J.; Otyepka M. MOLEonline: a web-based tool for analyzing channels, tunnels and pores (2018 update). *Nucleic Acids Res* **2018,** *46(W1),* W368–W373
71. Kozakov D.; Hall D.R.; Xia B.; Porter K.A.; Padhorny D.; Yueh C.; Beglov D.; Vajda S. The ClusPro web server for protein-protein docking. *Nature Protocols* **2017,** *12(2),* 255-278\
72. Krissinel E.; Henrick K. Inference of macromolecular assemblies from crystalline state. *J Mol Biol* **2007,** *372,* 774-797
73. Morris G.M.; Huey R.; Lindstrom W.; Sanner M.F.; Belew R.K.; Goodsell D.S.; Olson A.J. Autodock4 and AutoDockTools4: automated docking with selective receptor flexiblity. *J Comput Chem* **2009,** *16,* 2785-2791
74. Sanner M.F. Python: A Programming Language for Software Integration and Development. *J Mol Graphics Mod* **1999,** *17,* 57-61
75. Pauliukaite R.; Brett C.M.A. Poly(neutral red): Electrosynthesis, Characterization, and Application as a Redox Mediator. *Electroanalysis* **2008,** *20(12),* 1275-1285
76. Sadowski J.; Gasteiger J.; Klebe G. Comparison of Automatic Three-Dimensional Model Builders Using 639 X-Ray Structures. *J Chem Inf Comput Sci* **1994,** *34,* 1000-1008
77. Trott O.; Olson A.J. AutoDock Vina: improving the speed and accuracy of docking with a new scoring function, efficient optimization, and multithreading. *J Comput Chem* **2010,** *31(2),* 455-461
78. Sumaryada T.; Sandy Gunawan M.; Perdana S.; Arjo S.; Maddu A. A Molecular Interaction Analysis Reveals the Possible Roles of Graphene Oxide in a Glucose Biosensor. *Biosensors (Basel),* **2019,** *9(1),* E18